Nucleic Acids Research, 2025, **53**, gkaf704
https://doi.org/10.1093/nar/gkaf704
Genome integrity, repair and replication

Recombination-coupled DNA synthesis facilitates post-invasion steps in meiotic crossover and noncrossover formations

Hyungseok Choi[†], **Jun Seo Lee**[†], **Jeong H. Joo, Soogene Lee, Keun P. Kim** *

Department of Life Sciences, Chung-Ang University, Seoul 06974, South Korea

*To whom correspondence should be addressed. Email: kpkim@cau.ac.kr
[†]The first two authors should be regarded as joint first authors.

Abstract

During meiotic double-strand break (DSB) repair, most DSBs undergo tightly regulated 5′ end resection, generating 3′ single-stranded (ss) DNA tails, which assemble Rad51 and Dmc1 filaments to facilitate homology search and strand exchange for recombination. However, the occurrence of local DNA synthesis at the 3′ end of the ssDNA in DSBs concerning the majority crossover and noncrossover processes at the DNA level and the involvement of DNA polymerase at the recombination site have remained unclear. Here, we investigated meiotic recombination-coupled DNA synthesis (MRDS) in *Saccharomyces cerevisiae* through a physical analysis of recombination events, timed incorporation of thymidine analogs, and super-resolution microscopy imaging. We demonstrate that DNA polymerase δ (Pol δ) is required to extend the initial D-loop through its end-primed synthesis activity. Importantly, Pol δ-mediated MRDS facilitates post-invasion steps for both double Holliday junction and noncrossover formations. We infer that MRDS is required for displacement-loop/single-end invasion extension through end-primed synthesis, ensuring accurate base pairing between the leading and complementary strands. This study highlights the critical role of Pol δ in MRDS and illustrates the robust regulation of recombination during the post-invasion stages.

Graphical abstract

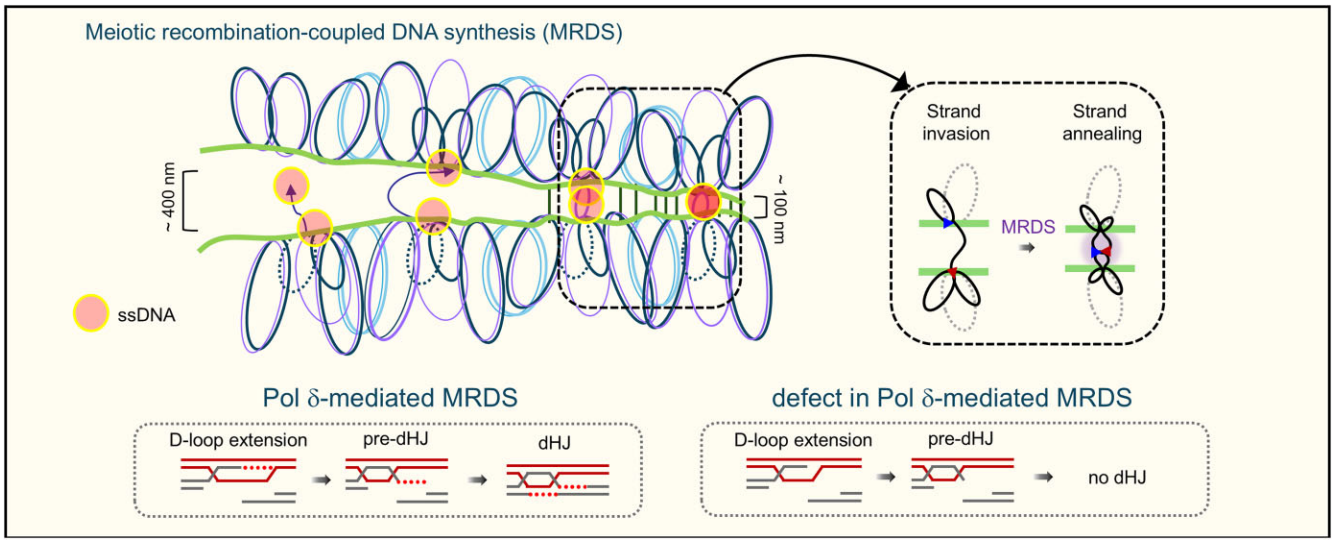

Introduction

Recombination is an important feature in meiosis and creates genetic diversity through an exchange of DNA between maternal and paternal chromosomes [1]. Additionally, recombination is essential in chromosome pairing and homologous chromosome segregation during meiosis [2, 3]. In most eukaryotic organisms, recombination commences with meiosis-specific DNA double-strand breaks (DSBs), which are initiated in early prophase by a meiosis-specific transesterase protein, Spo11, along with its associated proteins [4–6].

Budding yeast studies revealed that strands with 5′ ends at the DSB sites are then processed by Mre11/Rad50/Xrs2

Received: December 16, 2024. **Revised:** July 3, 2025. **Editorial Decision:** July 6, 2025. **Accepted:** July 8, 2025

plus Sae2 and Exo1–Sgs1 activity to expose 3′ single-stranded tails that can subsequently function as the leading strand for recombination-coupled DNA synthesis and D-loop extension with a homolog duplex DNA [7–11]. DSB end resection typically results in an average length of ∼800 nucleotides, with over 90% of DSBs undergoing resection of at least 500 nucleotides [11]. DNA synthesis is required following DSB resection to repair the generated long 3′ single-stranded DNA ends [12]. This synthesis facilitates the processing of recombination intermediates and forms heteroduplex DNA during meiotic prophase I, a particularly important process between zygotene and pachytene [10, 13]. RecA homologs, Dmc1 and Rad51, and their accessory proteins mediate meiotic DSB repair via recombination through a partner homologous chromosome template [14, 15]. Rad51 is assisted in this process by accessory factors ("mediators") [14–16]. Conversely, Dmc1, the meiosis-specific homolog of Rad51, performs the strand exchange during programmed meiotic recombination [14]. Further, Dmc1 has its own set of meiosis-specific mediator factors, including Mei5–Sae3, Hop2–Mnd1, and Tid1/Rdh54 [17–20]. In the yeast crossover (CO) pathway, facilitated by the ZMM proteins (Zip1/Zip2/Zip3/Zip4, Mer3, Msh4/Msh5), the nascent D-loop is converted into a single-end invasion (SEI) [and "pre-double Holliday junction (pre-dHJ)"], in which the leading DSB end has undergone strand exchange and DNA synthesis with a partner duplex DNA (Fig. 1A) [10, 21–25]. The SEI can then capture the "second" DSB end released from the quiescence complex on the sister chromatids and transmit it to the double Holliday junction (dHJ) (Fig. 1A) [21]. Similar strand exchange/DNA synthesis/extension patterns occur in the noncrossover (NCO) pathway (Fig. 1A) [24]. However, branch migration mediated by helicase promotes the disassembly of an extended D-loop, followed by second-end annealing to form the NCO [22–25]. Both Rad52 and replication protein A (RPA) are significantly important in facilitating the efficient progression of interactions directed towards the CO and NCO formations during the second strand annealing steps [26, 27].

Saccharomyces cerevisiae DNA Pol δ, which contains three catalytic subunits (Pol3, Pol31, and Pol32), is involved in synthesizing the DNA lagging strand, in addition to contributing to leading-strand DNA synthesis in DNA repair and replication [28]. Similar to yeast Pol δ, the human Pol δ enzyme comprises four subunits (POLD1–4), with POLD1 being the largest (124 kDa). Moreover, POLD1 possesses both catalytic polymerase activity and a proofreading 3′–5′ exonuclease function during DNA replication and recombination [29, 30]. Previous studies have indicated that Pol δ is the primary polymerase responsible for high-fidelity DNA synthesis during recombination [31–36]. Roeder *et al.* investigated the role of Pol δ during meiosis in *S. cerevisiae* [31], performing an extensive screening for meiotic recombination mutants, which led to the identification of *pol3-ct*, a variant characterized by a shortened terminal truncation (missing the last four amino acids, LSKW) in the Pol δ catalytic subunit [31]. Genetic analysis of the *pol3-ct* mutation demonstrated that Pol δ is crucial for determining the tract length of the gene conversion and CO formation in meiosis. They further proposed that Pol δ increases the length of heteroduplex DNA by facilitating DNA synthesis, which is coupled with the extended removal of the resected strand, either through strand displacement or additional 5′ to 3′ resection [31]. Recombination fundamentally relies on the essential process of end-primed DNA synthesis within the transient D-loop, which is critical for initiating the exchange of genetic material between homologous chromosomes. This process is necessary for generating the intermediate structures required for recombination, including the formation of heteroduplex DNA. Consequently, Pol δ may play a key role in extending the D-loop, particularly through synthesizing the DNA on the 3′ ends of the leading strand (DNA synthesis tracts) during meiosis (Fig. 1A). Without efficient DNA synthesis, the recombination process would be impaired, potentially leading to incomplete or faulty genetic exchange. Multiple studies have defined meiotic DSB formation and recombination processes by presenting evidence of strand invasion and extensive branch migration in the D-loop/SEI structure [22, 25, 37]. However, knowledge of the specific mechanisms and regulatory proteins involved in local DNA synthesis at the recombination interaction site of paired chromosomes *in vivo* remains limited. Thus, this study aimed to investigate a major meiotic recombination-coupled DNA synthesis (MRDS) process concerning recombination-mediated DSB repair and the arrangement of single-stranded DNA (ssDNA) on paired chromosomes during prophase.

This study identified the precise roles of DNA polymerases in the post-invasion stage of meiotic recombination, specifically focusing on the function of Pol δ during prophase I. Our results show that Pol δ is crucial for extending the 3′ ssDNA end that invades the homologous duplex, a step essential for both CO and NCO formations. We found that Pol δ facilitates the maintenance of homologous chromosome interactions during recombination by catalyzing the extension of the invading strand. In contrast, Pol ε did not possess a significant role in this process. Using budding yeast, we defined the mechanism of MRDS and directly visualized recombination intermediates. Moreover, by incorporating thymidine analogs to track DNA synthesis during prophase I, we obtained detailed insights into the dynamics of post-invasion DNA synthesis, providing further evidence of the role of Pol δ in extending the invading strand. Additionally, we revealed that an RPA fraction persists on the outer sides of the chromosome axes following Pol δ depletion, whereas Zip3 is normally localized to CO-designated sites. Based on these findings, we suggest a fundamental mechanism through which local DNA synthesis occurs at DSB sites, implying that a relationship exists between MRDS and post-invasion steps concerning meiotic CO and NCO recombination.

Materials and methods

Strains

All yeast strains used in the experiment are *S. cerevisiae* SK1 derivatives. Detailed information on genotypes is described in Supplementary Table S1. The insertion of the *HIS4LEU2* locus has been described previously [38, 39].

Synchronous meiosis time course

Synchronous meiosis was executed as described previously [21, 27, 38–45]. Yeast diploid cells stored at −80°C were inoculated onto YPG agar plates (1% yeast extract, 2% Bacto-peptone, 2% Bacto-agar, and 3% glycerol) and incubated at 30°C for 16 h. The grown cells were diluted on YPD agar plates (1% yeast extract, 2% Bacto-peptone, 2% Bacto-agar,

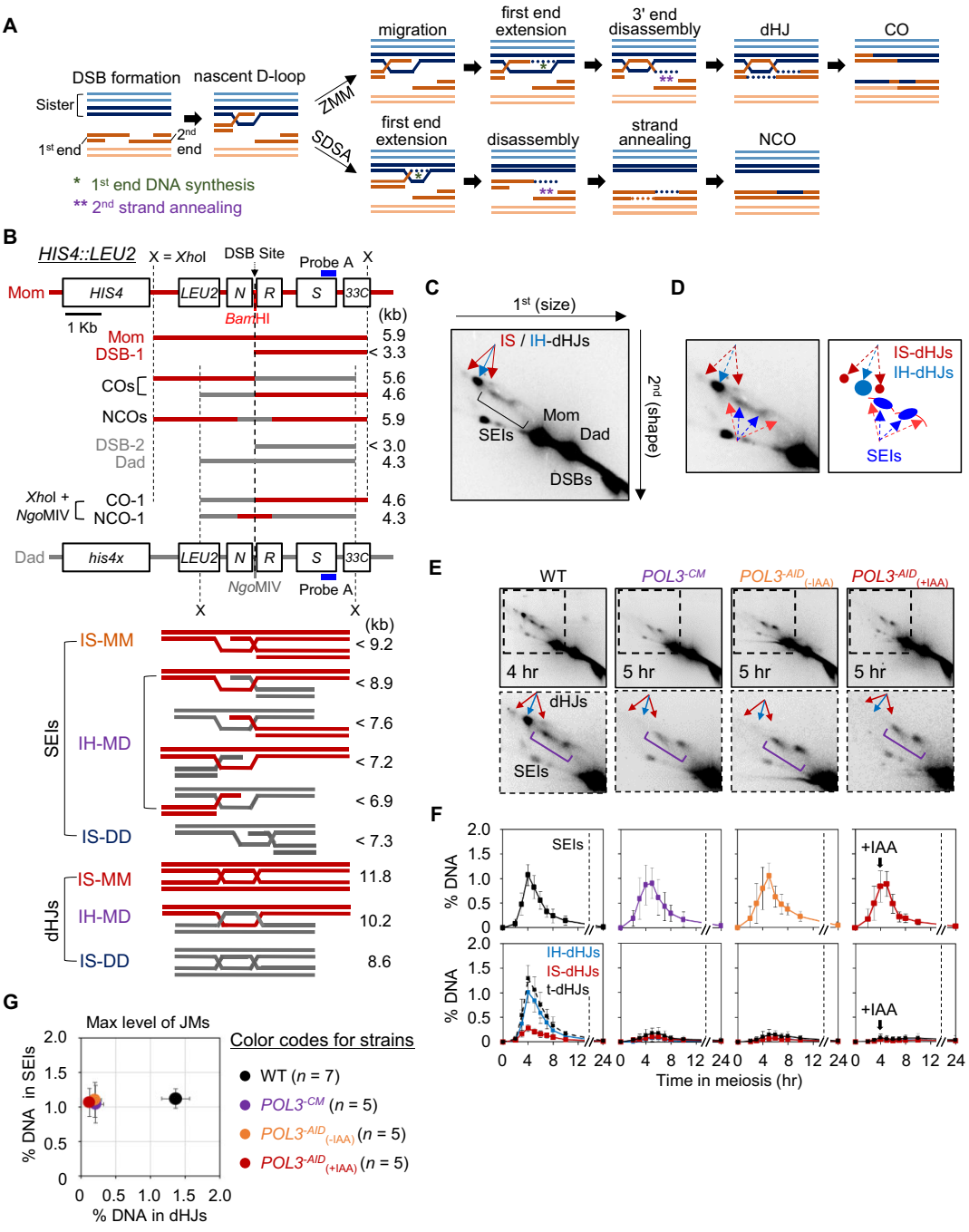

Figure 1. DNA Pol δ is required to form dHJs. (**A**) Consensus model for DNA synthesis and strand annealing in meiotic recombination. In the yeast CO recombination, a nascent D-loop forms and transforms into a SEI species. In this process, the leading strand in a DSB undergoes strand invasion and DNA synthesis with a complementary strand from a partner duplex [23, 25]. The SEI can subsequently engage with the second DSB end, which is released from the sister chromatids, ultimately guiding the end towards the formation of a dHJ [21]. A similar series of events, e.g. strand invasion, DNA synthesis, and extension, also occurs in the NCO pathway through SDSA [24]. (**B**) Map of the physical analysis at the *HIS4LEU2* locus in chromosome 3 shows the XhoI restriction enzyme sites and probe A position for Southern blot hybridization. XhoI restriction enzyme site polymorphisms distinguish DNA species between paternal and maternal DNA. Dad, paternal species (4.3 kb); mom, maternal species (5.9 kb); DSBs (3.3 and 3 kb); COs (5.6 and 4.6 kb); NCOs (5.9 and 4.3 kb). The SEIs are differentiated as IS-MM, intersister maternal species (<9.2 kb); IH-MD, interhomolog maternal and paternal species (<8.9 kb, <7.6 kb, <7.2 kb, and <6.9 kb); IS-DD, intersister paternal species (<7.3 kb). The dHJs are distinguished as IS-MM, intersister maternal species (11.8 kb); IH-MD, interhomolog maternal and paternal species (10.2 kb); IS-DD, intersister paternal species (8.6 kb), respectively. XhoI and NgoMIV restriction enzymes were used to distinguish between CO-1 and NCO-1, respectively. (**C**) Representative two-dimensional (2D) gel image. (**D**) Diagram of JMs. The dHJs are indicated by red arrows (IS-dHJ) or blue arrows (IH-dHJs). (**E**) Two-dimensional gel analysis of JMs in WT, *POL3*$^{-CM}$, *POL3*$^{-AID}_{(-IAA)}$, and *POL3*$^{-AID}_{(+IAA)}$ cells. The dashed box shows the enlargement of JMs. (**F**) Quantification of JMs throughout meiosis. Data are presented as the average ± SD ($n = 7$ for WT; $n = 5$ for *POL3*$^{-CM}$, *POL3*$^{-AID}_{(-IAA)}$, and *POL3*$^{-AID}_{(+IAA)}$). Cells were cultured in the absence (- auxin) or presence of IAA (+ auxin). The t-dHJs label refers to total dHJs. (**G**) Average levels of SEIs and dHJs from multiple 2D gel analyses in WT, *POL3*$^{-CM}$, *POL3*$^{-AID}_{(-IAA)}$, and *POL3*$^{-AID}_{(+IAA)}$ cells. SEIs and dHJs are indicated as a percentage of maximum levels. Data are presented as the average ± SD. "*n*" refers to the number of biological replicates in the experiments.

and 2% dextrose) and incubated at 30°C for 2 days to acquire single colonies. A single colony was inoculated into 2 ml of YPD liquid medium and incubated at 30°C for 24 h with gentle shaking until saturation. To synchronize cells at the G_1-phase in the cell cycle, saturated cultures were diluted in SPS medium (0.5% yeast extract, 1% Bacto-peptone, 0.17% yeast nitrogen base without amino acids, 0.5% ammonium sulfate, 1% potassium acetate, 50 mM potassium hydrogen phthalate, and adjusted to pH 5.5 using KOH), then incubated at 30°C for 17 h with gentle shaking. Meiosis was initiated by transferring the SPS-cultured cells to an SPM medium (1% potassium acetate, 0.02% raffinose, and 0.01% antifoam). Then, these SPM-cultured cells were harvested at 0, 2.5, 3.5, 4, 5, 6, 7, 8, 10, and 24 h. Next, $CuSO_4$ (20 μM) and auxin (2 mM) were added to the SPM-cultured cells at 3.5 and 4 h post-meiosis induction, respectively, to promote auxin-induced degradation of Pol ε (Pol2) and Pol δ (Pol3 and Pol31), respectively. To analyze meiotic division, cells were resuspended with a fixation solution (40% ethanol and 0.1 M sorbitol) and observed microscopically using DAPI (4′,6-diamidino-2-phenylindole) staining.

Physical analysis of recombination

Yeast genomic DNA was prepared using the previously described guanidine–phenol extraction method [14, 27, 41–45]. Cells were harvested from the SPM culture and resuspended in spheroplasting buffer (1 M sorbitol, 50 mM potassium phosphate, 0.4 mg/ml lyticase, 1% β-mercaptoethanol, and 10 mM EDTA) and incubated at 37°C to react. Spheroplast cells were resuspended in guanidine–HCl solution (4.5 M guanidine–HCl, 0.1 M EDTA, 0.15 M NaCl, 0.05% sodium lauroyl sarcosinate, and adjusted to pH 8.0 using NaOH) at 65°C. The lysates were precipitated using ethanol and administered RNase A [10 mM Tris (pH 8.0), 10 mM EDTA (pH 8.0), and 50 μg/ml RNase A] and proteinase K. Genomic DNA was extracted using phenol/chloroform/isoamyl alcohol (25:24:1) solution and precipitated in ethanol. For one-dimensional (1D) gel electrophoresis analysis, 2 μg of genomic DNA was digested with XhoI and/or NgoMIV at 37°C. Digested genomic DNA was electrophoresed at 2 V/cm in 0.6% UltraKem LE agarose gel. For two-dimensional (2D) gel electrophoresis analysis at various chromosome loci, 2.5 μg of genomic DNA was digested with XhoI for the *HIS4LEU2* locus, BglII for the *ARG4* locus, and HindIII for the *BUD23*, *CYS3*, and *ERG1* loci. Digested genomic DNA was fractionated by electrophoresis at 1 V/cm in 0.4% SeaKem Gold agarose. The gels were stained with 0.5 μg/ml ethidium bromide (EtBr), and the gel strips were placed perpendicular and electrophoresed at 6 V/cm in a 0.8% UltraKem LE agarose gel. To analyze COs and NCOs using 2D gel electrophoresis, 2 μg of XhoI-digested genomic DNA was electrophoresed at 2 V/cm in 0.6% SeaKem Gold agarose. The gel was stained using 0.5 μg/ml EtBr in 10 mM Tris (pH 8.0) and sliced between 7 and 2.5 kb. The gel strips were digested using BamHI and washed in TBE buffer [89 mM Tris (pH 8.0), 89 mM boric acid, and 2 mM EDTA], then electrophoresed at 6 V/cm in a 0.7% UltraKem LE agarose gel. The gel was transferred to a Biodyne membrane (Pall), and α-^{32}P–dCTP (Revvity, PK-BLU013H)-radiolabeled probes were used to detect DNA species. These DNA species were visualized and quantified using the Personal Molecular Imager system (Bio-Rad) with Quantity One software (Bio-Rad).

Spot-test and spore viability

Single colonies of diploid strains were inoculated into 2 ml of YPD liquid medium and incubated at 30°C for 24 h. Saturated cells ($OD_{600} = 1.0$) were serially diluted ten-fold in YPD liquid medium and spotted onto YPD and IAA plates (20 μM $CuSO_4$ and 2 mM auxin). For the spore viability analysis, diploid cells were cultured in an SPM medium at 30°C overnight. Each of the four haploid spores derived from tetrad cells was isolated on a YPD plate using a micromanipulator device (Singer) and grown at 30°C for 2 days. The spore viability was assessed as the number of surviving spores per tetrad of at least 100 for reliable evaluation.

Chromosome spreading

Chromosomal spreading preparations for the immunofluorescence analysis were performed as previously described [17, 27, 41, 42, 44, 46]. The cells were harvested at each time point and resuspended in ZK buffer containing Dithiothreitol [50 mM Tris (pH 7.5), 0.5 M KCl, and 25 mM Dithiothreitol]. This suspension was left at room temperature for 2 min. Subsequently, a lyticase (Sigma, L4025-250KU) solution [5% glucose, 50 mM Tris (pH 7.5), and lyticase] was added to lyse the yeast cell wall, and the mixture was placed in a shaking incubator. The harvested cell pellets were then washed with chilled MES wash solution [1 M sorbitol, 0.1 M MES, 1 mM EDTA, and 0.5 mM $MgCl_2$ (pH 6.5)]. Yeast cells were fixed using a cross-linking solution (3% paraformaldehyde and 3.4% sucrose) and 1% Lipsol (Scilabware, Py.40023). Afterward, the lysed cells were spread onto clean slides and left overnight to ensure thorough drying.

BrdU and EdU incorporation assays

As previously described, *S. cerevisiae* cannot use bromodeoxyuridine (BrdU) in DNA synthesis due to the absence of a thymidine salvage pathway; however, BrdU can be used in *S. cerevisiae* through the additional expressions of *Herpes simplex* virus thymidine kinase (*HSV-TK*) and human equilibrative nucleoside transporter (*hENT1*) [10, 47, 48]. Thus, to construct strains for BrdU incorporation, *HSV-TK*, and *hENT1* genes in the p306–BrdU–Inc plasmid were amplified via polymerase chain reaction (PCR) and inserted into the *URA3* locus [48]. To detect newly synthesized DNA in meiotic chromosomes after inducing meiosis in SPM, yeast diploid cells were treated with 200 μg/ml BrdU (#B5002, Sigma) for 1 h (2–3, 3–4, 4–5, and 5–6 h) or 2 h (0–2 h) before cell harvesting (Fig. 4A). For 5′-ethynyl-2′-deoxyuridine (EdU) incorporation to perform microscopy analyses, cells were treated with 100 μg/ml EdU (#C10340, Invitrogen) for 2 h. A click-iT reaction was conducted by adding a reaction cocktail (manufacturer's composition) to each slide at room temperature for 30 min. The chromosomal DNA was spread using a previously described method [17, 27, 41, 42, 44, 46]. The BrdU- or EdU-labeled cell spread slides were added to 0.2% Photo-Flo (Kodak) for 30 s to remove the sucrose coating and washed in Tris-Buffered Saline (TBS) buffer [25 mM Tris (pH 7.5), 136 mM NaCl, and 3 mM KCl] for 15 min. To perform the BrdU incorporation microscopy assay, slides were placed in 4 M HCl for 5 min to denature meiotic DNA and washed in TBS buffer for 15 min. Then, labeled slides were washed with TBS containing 1% Bovine serum albumin (BSA). Before primary antibody treatment, slides were blocked by

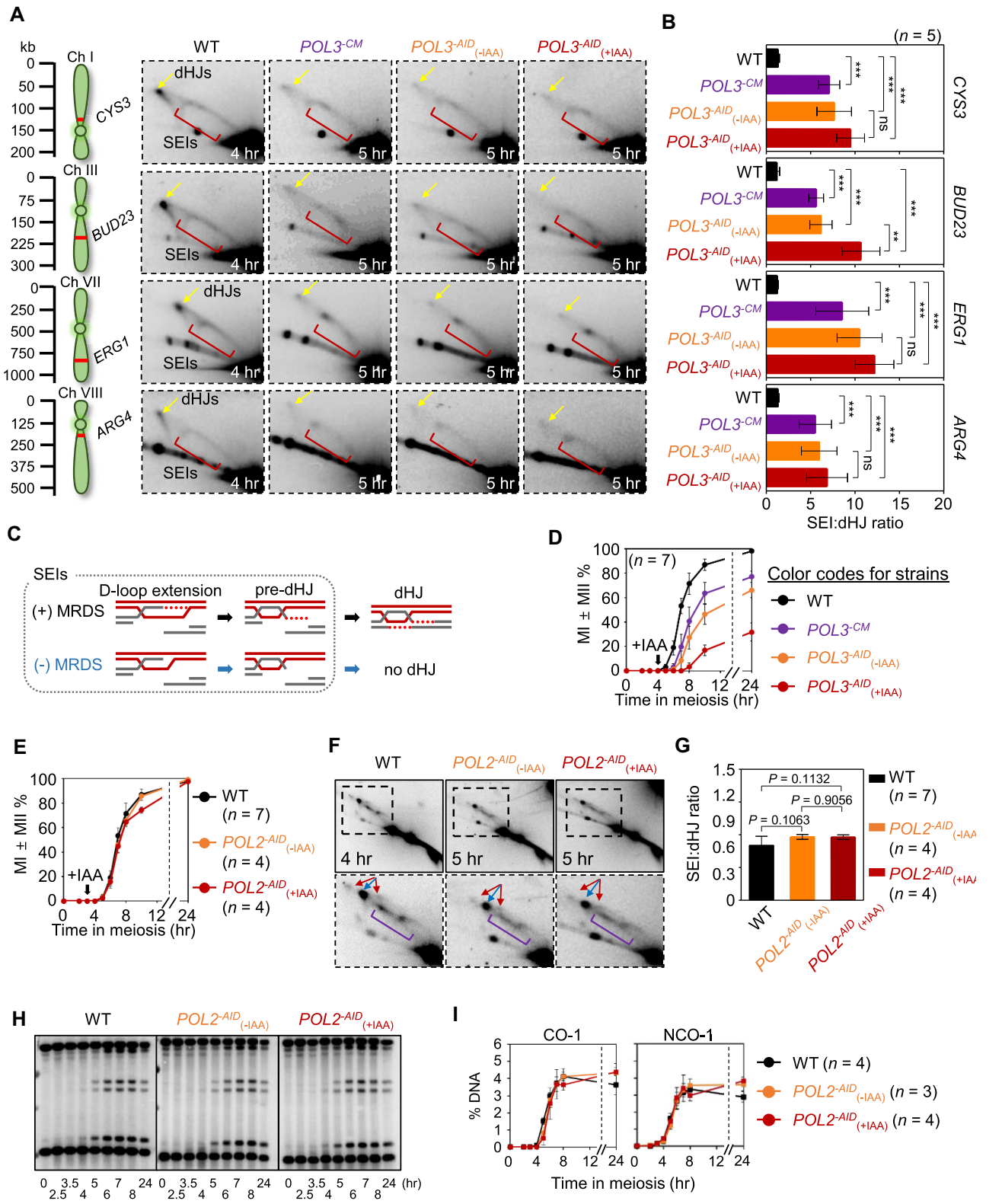

Figure 2. DNA Pol δ activity promotes SEI-to-dHJ transition. (**A**) Analysis of JMs in WT, *POL3*$^{-CM}$, *POL3*$^{-AID}_{(-IAA)}$, and *POL3*$^{-AID}_{(+IAA)}$ cells at various loci (*CYS3*, *BUD23*, *ERG1*, and *ARG4*). (**B**) Ratio of SEI:dHJ plotted as a percentage of the maximum level. Data are presented as the average ± SD ($n = 5$). Statistical significance was assessed using an unpaired *t*-test to compare WT and *pol3* mutants with and without IAA treatment in *POL3*$^{-AID}$ cells. **P < 0.01; ***$P < 0.001$; and ns = not significant. (**C**) Schematic comparing MRDS (+) and MRDS (-) for the SEI-to-dHJ transition. (**D**) Meiotic division analysis of *pol3* mutants. Error bars represent the average ± SD ($n = 7$ for all strains). (**E**) Analysis of meiotic division for *pol2* mutants. Error bars represent the average ± SD ($n = 7$ for WT from Fig. 2D; $n = 4$ for *POL2*$^{-AID}_{(-IAA)}$ and *POL2*$^{-AID}_{(+IAA)}$). (**F**) Analysis of the SEIs and dHJs in WT, *POL2*$^{-AID}_{(-IAA)}$, and *POL2*$^{-AID}_{(+IAA)}$ cells. WT image from Fig. 1E. (**G**) Ratio of SEI:dHJ plotted as a percentage of the maximum level. WT data from Fig. 1G. Data are presented as the average ± SD ($n = 7$ for WT; $n = 4$ for *POL2*$^{-AID}_{(-IAA)}$ and *POL2*$^{-AID}_{(+IAA)}$). Statistical analysis was performed using an unpaired *t*-test to compare WT and *pol2* mutants. "*n*" refers to the number of biological replicates. (**H**) Representative images of CO and NCO analysis in WT, *POL2*$^{-AID}_{(-IAA)}$, and *POL2*$^{-AID}_{(+IAA)}$ cells. (**I**) Quantification of COs and NCOs in indicated strains. "*n*" refers to the number of biological replicates.

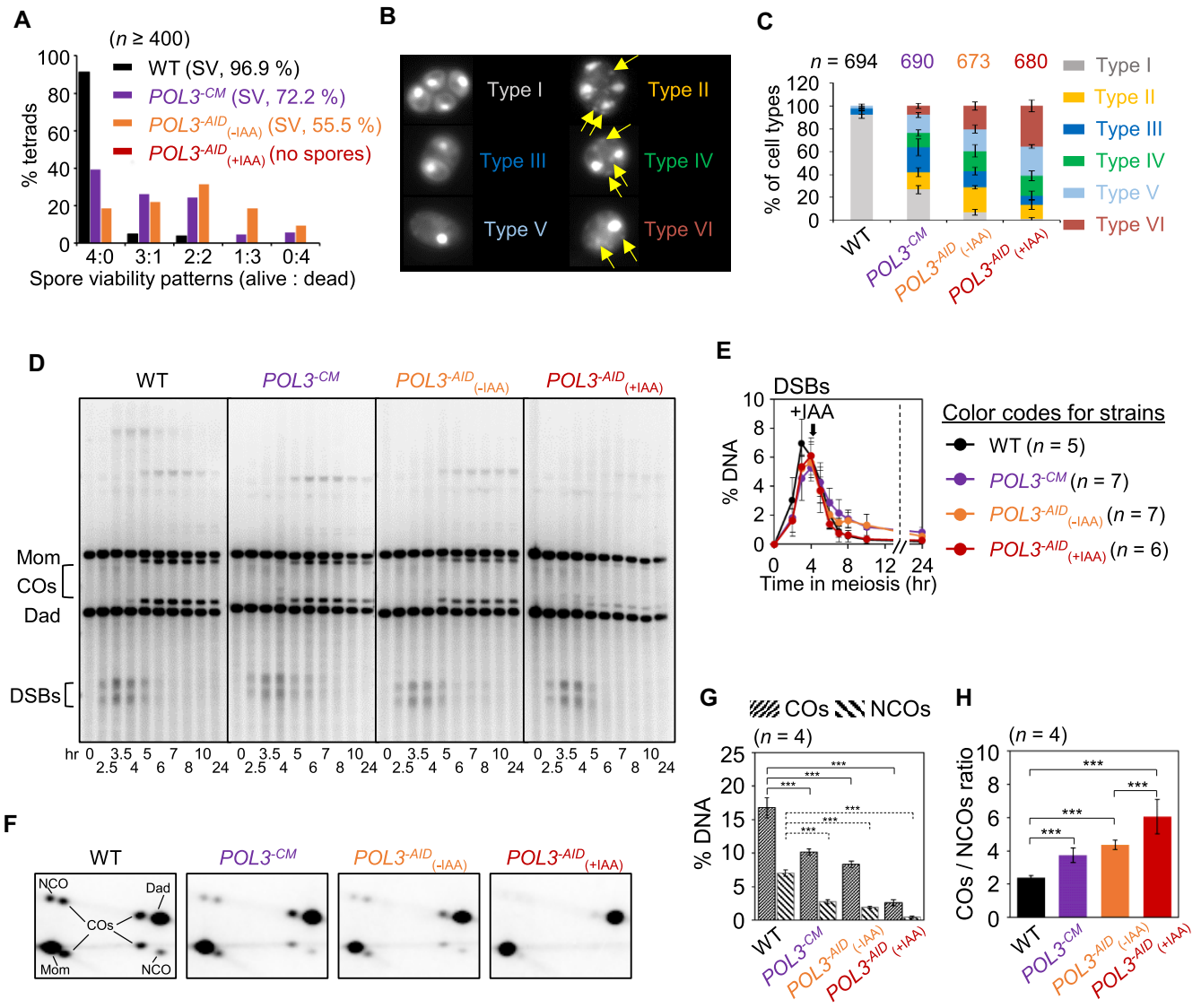

Figure 3. *POL3*$^{-CM}$ and *POL3*$^{-AID}$ cells exhibit meiotic catastrophe and recombination defects. (**A**) Spore viability analyses for WT, *POL3*$^{-CM}$, *POL3*$^{-AID}_{(-IAA)}$, and *POL3*$^{-AID}_{(+IAA)}$ cells. The horizontal axis represents the number of viable spores per tetrad, while the vertical axis represents the percentage of tetrad class. The value of "*n*" represents the number of spores. (**B**) Representative cells from WT, *POL3*$^{-CM}$, *POL3*$^{-AID}_{(-IAA)}$, and *POL3*$^{-AID}_{(+IAA)}$ cells at 24 h after meiosis induction. DAPI-stained images depict the same cells classified into six types: Type I (tetrad cell), Type II (tetrad cell with broken DNAs), Type III (dyad cell), Type IV (dyad cell with broken DNAs), Type V (monad cell), and Type VI (monad with broken DNAs). Yellow arrows indicate unsegregated DNA masses. (**C**) Quantification of cell types. Bar colors indicate Type I (gray), Type II (yellow), Type III (blue), Type IV (green), Type V (sky blue), and Type VI (brown). The value of "*n*" represents the number of cells. (**D**) One-dimensional (1D) gel analysis in WT, *POL3*$^{-CM}$, *POL3*$^{-AID}_{(-IAA)}$, and *POL3*$^{-AID}_{(+IAA)}$ cells. COs, crossovers; DSBs, double-strand breaks. (**E**) Quantitative analysis of DSBs in WT, *POL3*$^{-CM}$, *POL3*$^{-AID}_{(-IAA)}$, and *POL3*$^{-AID}_{(+IAA)}$ cells. Data are presented as the average ± SD ($n = 5$ for WT; $n = 7$ for *POL3*$^{-CM}$ and *POL3*$^{-AID}_{(-IAA)}$; $n = 6$ for *POL3*$^{-AID}_{(+IAA)}$). (**F**) Two-dimensional gel analysis of COs and NCOs in WT, *POL3*$^{-CM}$, *POL3*$^{-AID}_{(-IAA)}$, and *POL3*$^{-AID}_{(+IAA)}$ cells. (**G**) Quantitative analysis of COs and NCOs (8 h for WT and 24 h for *pol3* mutants). COs (an upward diagonal line) and NCOs (a downward diagonal line). (**H**) The ratio of COs and NCOs at the maximum value. Data are presented as the average ± SD ($n = 4$). The statistical significance was assessed using an unpaired *t*-test, comparing WT and *pol3* mutants with and without IAA treatment in *POL3*$^{-AID}$. The "*n*" number in Fig. 3E, G, and H refers to biological replicates; ***$P < 0.001$.

incubating in TBS containing 1% BSA in a wet chamber at room temperature for 30 min. Blocked slides were incubated in rat monoclonal anti-BrdU (diluted 1:500, Abcam, ab6326) antibody in a wet chamber at 4°C overnight. The secondary antibody fluorescein isothiocyanate-conjugated goat anti-rat IgG was used (diluted 1:500, Jackson ImmunoResearch, 112-095-003). Each slide was sealed with a mounting medium containing 1 μg/ml Hoechst 33342, and images were taken using a Nikon Eclipse Ti fluorescence microscope with a Nikon DS-Qi2 monochrome camera. The BrdU intensity was measured using ImageJ software.

Immunofluorescence N-SIM microscopy analysis

After being diluted in blocking buffer, primary antibodies were applied to the slides and incubated in a wet chamber at 4°C overnight. The primary antibodies used for immunostaining were as follows: mouse monoclonal anti-HA (diluted 1:200; Santa Cruz, sc-7392), rabbit polyclonal anti-Rfa1 (1:500; Agrisera, AS07214), rabbit polyclonal anti-Zip1 (diluted 1:500; custom), rat monoclonal anti-Myc (diluted 1:400; Bio rad, MCA1929), and mouse monoclonal anti-OctA (FLAG) (1:500; Santa Cruz, sc-166355). Subsequently, after the slides were immersed in TBST (TBS with

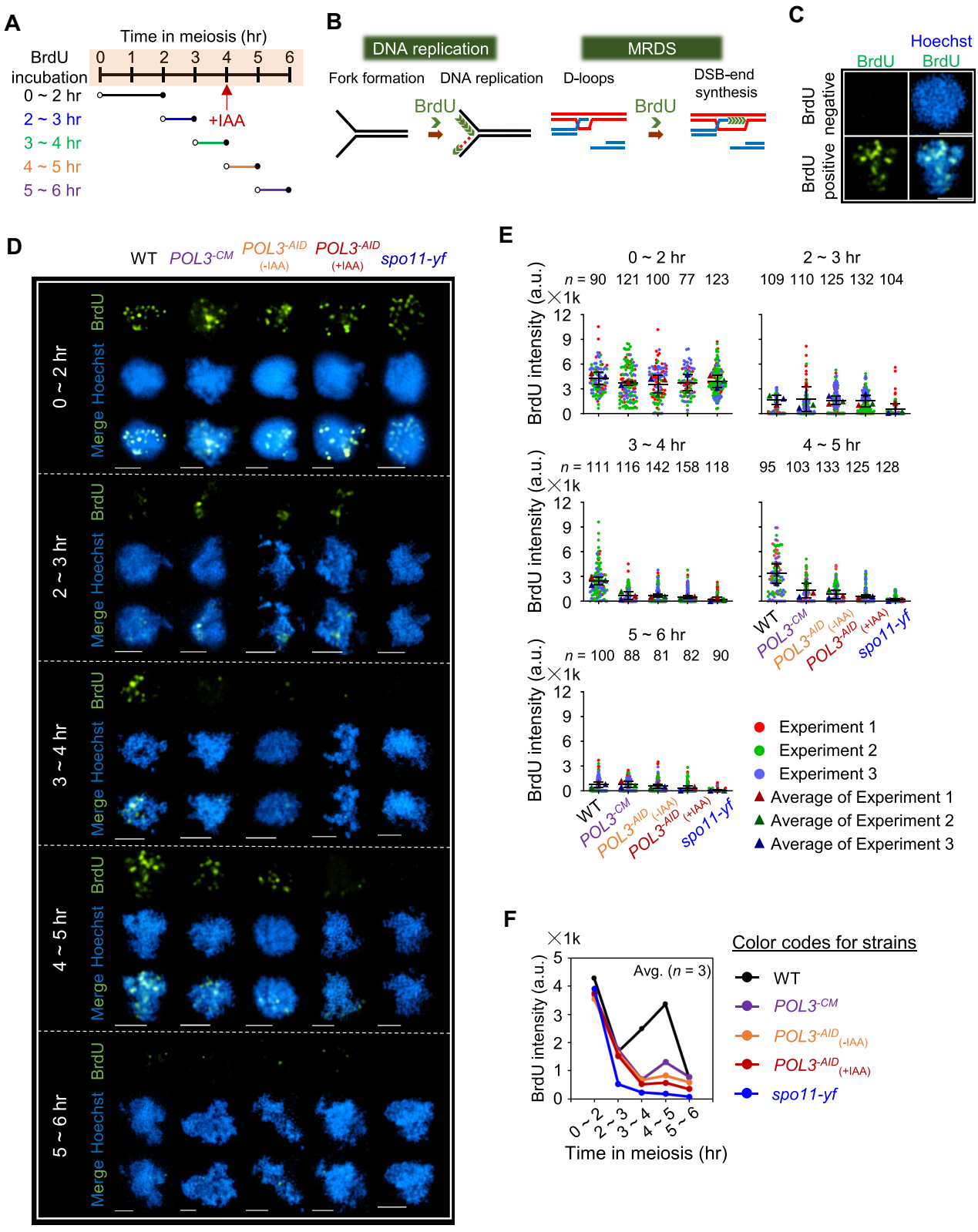

Figure 4. MRDS tracts by DNA polymerase δ in yeast chromosomal DNA. (**A**) Time schedule for detecting BrdU incorporation in meiotic chromosomal DNA. BrdU-labeling and sampling are indicated by open circles and filled circles, respectively. (**B**) Schematic of BrdU incorporation in DNA replication and MRDS. (**C**) Representative image of BrdU negative (absence of *HSV-TK* and *hENT1* genes) and positive (presence of *HSV-TK* and *hENT1* genes) nuclei. (**D**) Representative images of chromosomal DNA labeling with BrdU during the replication stage (0–2 and 2–3 h) and the subsequent MRDS stages (3–4, 4–5, and 5–6 h); scale bar: 2.5 μm. (**E**) The intensity of the BrdU signal in the meiotic chromosome. Superplots of BrdU intensities show the average of three independent experiment in triangles. "*n*" refers to the number of cells measured. (**F**) The intensity of BrdU signals in WT, *POL3*$^{-CM}$, *POL3*$^{-AID}_{(-IAA)}$, and *POL3*$^{-AID}_{(+IAA)}$ cells. Relative BrdU intensity was calculated by subtracting the BrdU intensity of *spo11-yf* from those in *SPO11 POL3* and *SPO11 pol3* mutants, respectively. a.u., arbitrary unit. "*n*" refers to the number of biological replicates.

0.1% Tween-20), secondary antibodies were added after being diluted in the same manner as above. The secondary antibodies used for immunostaining were as follows: Alexa-fluor-488-conjugated goat anti-mouse IgG (diluted 1:500; Jackson ImmunoResearch, 115-545-003), TRITC-conjugated goat anti-rabbit IgG (diluted 1:500; Jackson ImmunoResearch, 111-025-144), and Alexa-fluor-647-conjugated goat anti-rat IgG (diluted 1:500; Jackson ImmunoResearch, 112-605-003). Super-resolution images of chromosome spreads were acquired using an N-SIM microscope (Nikon Ti2-E, Tokyo, Japan) equipped with a DS-Qi2 monochrome camera (Nikon). The obtained image stack was reconstructed, and deconvolution was performed using NIS-Elements software.

Western blot

Yeast cells were resuspended in 0.3 M NaOH at room temperature for 5 min and then centrifuged at 5,000 rpm for 1 min. After discarding the supernatant, pellets were mixed with sodium dodecyl sulfate sample buffer [60 mM Tris (pH 6.8), 10% glycerol, 2% SDS, and 4% β-mercaptoethanol] and boiled for 5 min. The following antibodies were used: mouse monoclonal anti-Myc (diluted 1:5,000; Santa Cruz Biotechnology, sc-40), mouse monoclonal anti-Pgk1 (diluted 1:10,000; Novex, #459250), and HRP-conjugated goat anti-mouse IgG (diluted 1:5,000; Jackson ImmunoResearch, 115-035-003). Pgk1 was used as a loading control.

Cell cycle analysis

SPM cultured cells were resuspended in a fixation solution (40% ethanol and 0.1 M sorbitol) and then centrifuged at 5,000 rpm for 1 min. Pellets were treated with RNase A solution [50 mM Tris (pH 7.5) and 100 μg/ml RNase A] at 37°C for 1 h. Cells were sonicated for 10 s and then stained using 2 μg/ml propidium iodide (PI). Cell cycle analysis was performed using a BD Accuri™ C6 Plus Flow Cytometer and BD FACSCalibur™. Histograms of the cell cycle phases were visualized and quantified using BD Accuri C6 software, FlowJo™ v10.8 software, and ModFit LT™.

"SuperPlots" and statistical analysis

The BrdU intensity foci counts of RPA and Zip3 were analyzed to estimate the functional defects of *pol3* mutants using GraphPad Prism 10 software. The results are represented using "SuperPlots," which illustrate the full dataset distribution and provide statistical analyses to assess the reproducibility of the findings [49], as shown in Figs 4E, 5C, and 6B, D, and F. The average intensity values and foci numbers for each experiment are also presented as scatter plots, including the mean ± SD. Equal variances were assumed, and unpaired *t*-tests were performed to determine statistically significant differences between the means of multiple independent experiments or double mutant combinations.

Results

Deactivation of DNA polymerase δ *in vivo* via C-terminal tagging and controlled Pol3 degradation

Pol δ exists in *S. cerevisiae* as a heterotrimeric complex, which consists of a crucial Pol3 catalytic subunit and two additional accessory subunits: Pol31 and Pol32 (Supplementary Fig. S1A) [50]. Moreover, the Pol3 subunit in *S. cerevisiae* Pol δ is essential for normal growth [29]. To deplete DNA Pol3 during the meiotic cell cycle, we introduced a C-terminal auxin-inducible degron (AID) with a nine-Myc tag, allowing us to detect the presence of Pol3 (referred to as $POL3^{-AID}$) (Supplementary Fig. S1B). The Pol3 depletion in the $POL3^{-AID}$ strain, which possesses the plant F-box protein TIR1 that is capable of forming an active E3 ubiquitin ligase, was clearly detectable after treatment with indoleacetic acid (IAA) (Supplementary Figs S2A and B) [51, 52]. We then conducted a comparative analysis using a strain with a Pol3 incorporating a C-terminal nine-Myc tag ($POL3^{-CM}$). These *pol3* mutants were analyzed in parallel alongside the wild-type (WT). Both the $POL3^{-CM}$ and $POL3^{-AID}$ cells in the absence of auxin (designated as $POL3^{-AID}{}_{(-IAA)}$) grew normally but exhibited sensitivity to DNA damage, as observed in the serial dilution assays on medium containing methyl methane sulfonate (MMS) and hydroxyurea (HU) (Supplementary Fig. S2C). The C-terminal tag mutation associated with Pol3 likely affects the processivity of the enzyme by disrupting interactions with Pol31 and Pol32 (Supplementary Fig. S1A) [51]. However, a mitotic cell growth defect was observed following AID-induced degradation of Pol3 (designated as $POL3^{-AID}{}_{(+IAA)}$) (Supplementary Fig. S2C). Furthermore, the $POL3^{-CM}$ and $POL3^{-AID}{}_{(-IAA)}$ cells displayed a replication delay of ∼20 min before entering the G_2 phase, indicating that the reduced Pol δ activity may impair pre-meiotic replication (Supplementary Fig. S2D). Notably, adding auxin to $POL3^{-AID}$ cells at 4 h caused a pre-meiotic replication delay pattern similar to that observed in $POL3^{-AID}{}_{(-IAA)}$ cells (Supplementary Fig. S2C).

DNA polymerase δ is required to promote post-invasion steps

To understand the role of Pol δ in the DNA events in meiotic recombination, we monitored recombination intermediates at the *HIS4LEU2* locus on chromosome 3 using a physical analysis [14, 21, 38]. In WT meiosis, a DSB interacts with a partner and then, after a regulated differentiation, yields either a CO or a nonexchange NCO [24, 40]. Two successive stable branched intermediates are known to be included in a CO formation: The "first" DSB end interacts with its partner to create a SEI; then, after additional steps, the "second" DSB end is incorporated to form a dHJ (Fig. 1A) [21, 53, 54]. Both intermediates occur primarily between homologs rather than between sisters. For a specific, well-characterized recombination hotspot, i.e. *HIS4LEU2* (Fig. 1B), interhomolog and intersister species have different molecular weights and shapes (Fig. 1B); thus, these species can be distinguished at both the SEI and dHJ stages using diagnostic mobilities in native/native 2D gels (Fig. 1C and D).

Both mutants exhibited high SEI levels, comparable to those observed in the WT. However, the maximum dHJ levels were significantly reduced from 1.36% in WT cells to 0.21% and 0.20% in $POL3^{-CM}$ and $POL3^{-AID}{}_{(-IAA)}$ cells, respectively (Fig. 1E–G and Supplementary Fig. S3). Furthermore, the addition of auxin (IAA) to $POL3^{-AID}$ cells resulted in a reduction in dHJ levels (0.12%; Fig. 1E–G), similar to the defect observed in $POL3^{-AID}{}_{(-IAA)}$ cells. We further analyzed meiotic recombination at native DSB hotspots: *CYS3* locus (Chr 1), *BUD23* locus (Chr 3), *ERG1* locus (Chr 7), and *ARG4* locus (Chr 8). Similar to the joint molecule (JM) formation observed at the *HIS4LEU2* hotspot, WT SEI levels and

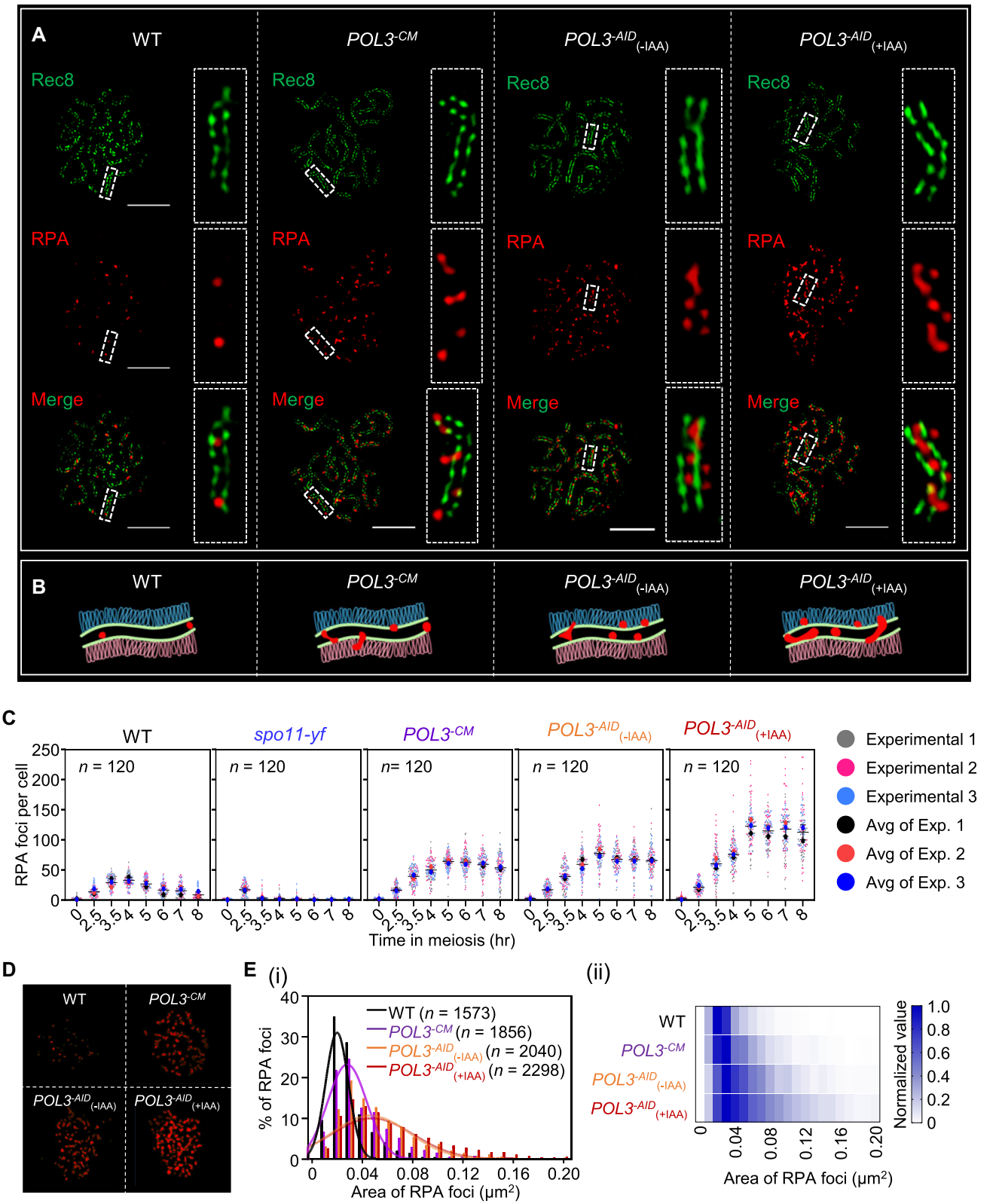

Figure 5. RPA–ssDNA filaments on the pachytene chromosomes are accumulated in *POL3*$^{-CM}$ and *POL3*$^{-AID}$ cells. (**A**) SIM images of replication protein A (RPA) and chromosome axis (Rec8) in zygotene and pachytene at 4 h for WT; 5 h for *POL3*$^{-CM}$; *POL3*$^{-AID}_{(-IAA)}$, and *POL3*$^{-AID}_{(+IAA)}$ cells: scale bar: 2.5 μm. (**B**) Cartoons of RPA long filaments induced by Pol δ inactivation in pachytene chromosomes. (**C**) Quantification of RPA foci numbers for WT, *POL3*$^{-CM}$, *POL3*$^{-AID}_{(-IAA)}$, *POL3*$^{-AID}_{(+IAA)}$, and *spo11-yf* cells. Superplots of the RPA foci numbers from three biological replicates ($n = 40$ for each experiment condition). Error bars indicate the standard deviation. (**D**) RPA-staining images for WT, *POL3*$^{-CM}$, *POL3*$^{-AID}_{(-IAA)}$, and *POL3*$^{-AID}_{(+IAA)}$ cells. Yellow lines delineate the outline of RPA. (**E**) RPA foci size distributions for WT, *POL3*$^{-CM}$, *POL3*$^{-AID}_{(-IAA)}$, and *POL3*$^{-AID}_{(+IAA)}$ cells. (**i**) The average numbers of RPA foci are quantified from three biological replicates ($n \geq 500$ for each experiment condition). Foci sizes were quantified using NIS element software. (**ii**) The heatmap indicates the distribution of the RPA foci sizes in WT, *POL3*$^{-CM}$, *POL3*$^{-AID}_{(-IAA)}$, and *POL3*$^{-AID}_{(+IAA)}$ cells.

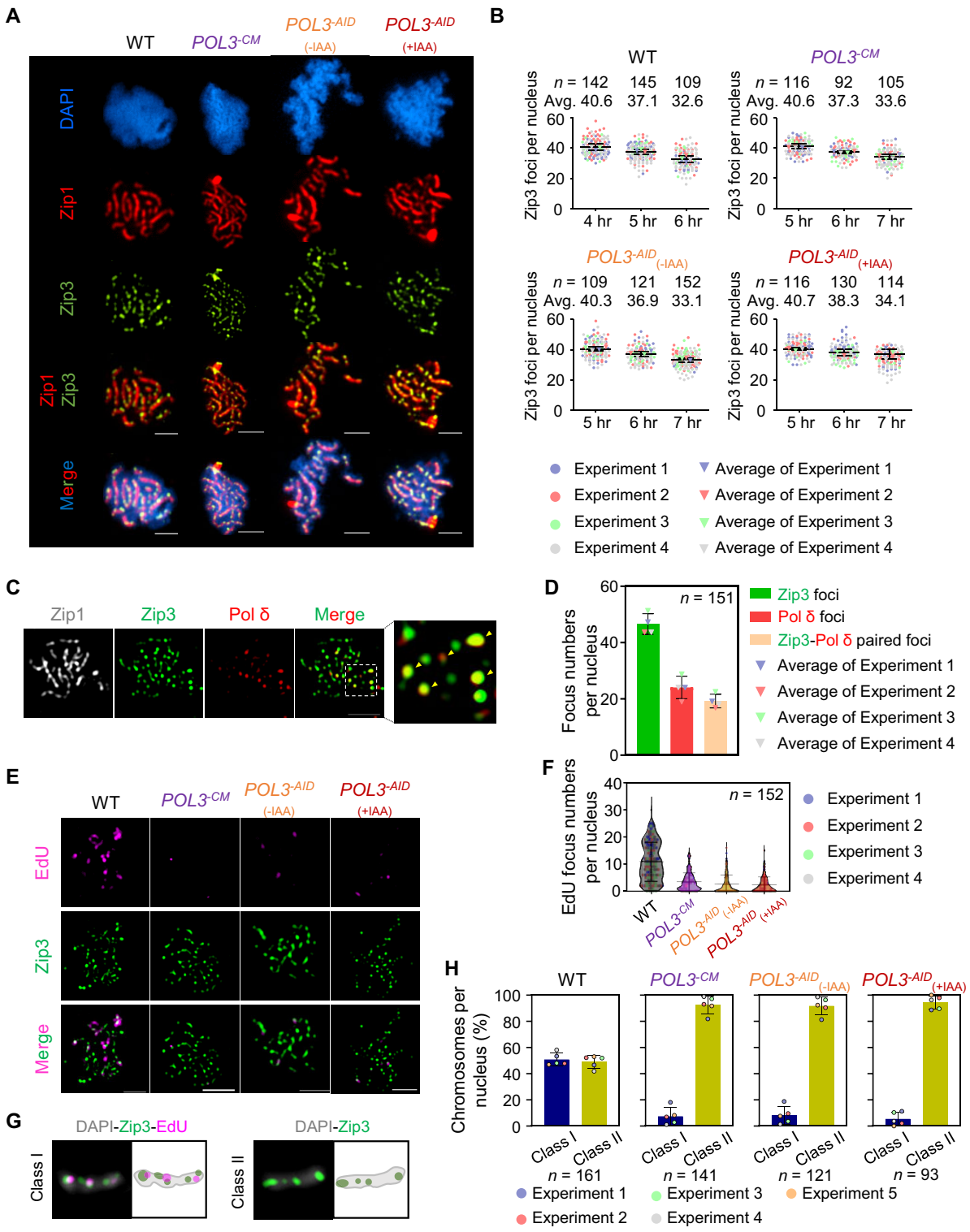

Figure 6. CO-designation and simultaneous SC nucleation occur independently of DNA synthesis. (**A**) Representative image of pachytene chromosomes stained for Zip1 and Zip3 in WT, *POL3*$^{-CM}$, *POL3*$^{-AID}_{(-IAA)}$, and *POL3*$^{-AID}_{(+IAA)}$ cells; scale bar: 2.5 μm. (**B**) Quantification of Zip3 foci in WT, *POL3*$^{-CM}$, *POL3*$^{-AID}_{(-IAA)}$, and *POL3*$^{-AID}_{(+IAA)}$ cells at the indicated times. Superplots of the numbers of Zip3 foci, with the average of each independent experiment indicated by a triangle ($n = 4$). Auxin (2 mM) was added to SPM-cultured cells 4 h after meiosis induction. (**C**) The Pol δ and Zip3 localization analysis was conducted by N-SIM microscopy in the pachytene stage (5 h). Yellow arrowheads indicate overlapping Pol δ–Zip3 foci; scale bar: 2.5 μm. (**D**) Quantification of Pol δ–Zip3 colocalization in the pachytene stage. The box plot indicates the average foci numbers from four biological replicates. (**E**) Representative images of meiotic pachytene showing EdU and Zip3 foci in WT, *POL3*$^{-CM}$, *POL3*$^{-AID}_{(-IAA)}$, and *POL3*$^{-AID}_{(+IAA)}$ cells (4–5 h for WT and 5–6 h for *pol3* mutants); scale bar: 2.5 μm. (**F**) Quantification of EdU foci numbers for WT, *POL3*$^{-CM}$, *POL3*$^{-AID}_{(-IAA)}$, and *POL3*$^{-AID}_{(+IAA)}$ cells (5 h for WT and 6 h for *pol3* mutants; $n = 4$). "*n*" refers to the number of biological replicates. (**G**) Cartoon of CO-associated DNA synthesis in pachytene chromosomes. (**H**) Quantification of Zip3–EdU staining (Class I and Class II in (G)) in WT, *POL3*$^{-CM}$, *POL3*$^{-AID}_{(-IAA)}$, and *POL3*$^{-AID}_{(+IAA)}$ cells; 5 h for WT and 6 h for *pol3* mutants ($n = 5$). "*n*" refers to the number of biological replicates. Error bars indicate the standard deviation. The values of "*n*" in Fig. 6B, D, F, and H represent the number of analyzed cells.

significant reductions in dHJs were also detected at the natural loci in *POL3*$^{-CM}$, *POL3*$^{-AID}$$_{(-IAA)}$, and *POL3*$^{-AID}$$_{(+IAA)}$ cells (Fig. 2A and B). Comparable results were observed following the Pol31 depletion (*POL31*$^{-AID}$$_{(+IAA)}$), a core subunit in Pol δ (Supplementary Figs S4 and S5). Thus, Pol δ-mediated DNA synthesis is not essential in SEI formations, but Pol δ activity might be directly involved in dHJ formation (Fig. 2C).

Pol ε foci were distributed throughout the nuclei in meiotic cells during prophase I (Supplementary Fig. S6A). To determine whether Pol ε was involved in meiotic DNA synthesis, we generated a degron-induced *POL2* knockdown allele by appending AID sequences to its C-terminus (*POL2*$^{-AID}$). The depletion of Pol2 by adding auxin to growth plates led to growth defects (Supplementary Fig. S6B). Similar to *POL3*$^{-AID}$ cells, *POL2*$^{-AID}$ cells without auxin treatment (-IAA) were able to undergo pre-meiotic DNA replication with a slight delay and continued through the meiotic cell cycle in a manner comparable to WT cells (Fig. 2D and E, and Supplementary Fig. S6C). Moreover, following auxin addition at 3.5 h, DSBs were induced in *POL2*$^{-AID}$$_{(+IAA)}$ cells and JM formation progressed similarly to that observed in *POL2*$^{-AID}$$_{(-IAA)}$ cells (Fig. 2F and G, and Supplementary Figs S6D and S7). Moreover, the CO and NCO products formed at comparable levels in WT cells (Fig. 2H and I). These findings suggest that Pol ε is not essential for promoting the transition from a SEI to a dHJ or NCO formation.

Meiotic catastrophe occurs in *POL3*$^{-CM}$ and *POL3*$^{-AID}$ cells

The timing and efficiency of nuclear divisions were monitored using DAPI staining. In WT cells, meiosis I (MI) was initiated ∼5 h after the cells were transferred to sporulation medium, followed by meiosis II (MII) (Fig. 2D). Meanwhile, ∼50% of the cells had completed one or both divisions (MI ± MII) at 7 h post-transfer. In contrast, normal nuclear divisions failed in the *POL3*$^{-CM}$ and *POL3*$^{-AID}$ cells, with 72.2% and 55.5% spore viabilities, respectively (Figs 2D and 3A). Consistent with these reduced spore viabilities, the *POL3*$^{-CM}$ and *POL3*$^{-AID}$ strains also displayed defects in completing meiotic divisions and spore formation (Figs 2D and 3A–C). Furthermore, *POL3*$^{-AID}$$_{(+IAA)}$ cells showed prophase I arrest with a single undivided nucleus or dyads, leading to an inability to form spores (Fig. 3A). Upon closer examination, a considerable proportion of the asci from both the *POL3*$^{-CM}$ and *POL3*$^{-AID}$$_{(-IAA)}$ cells contained DNA that had not been properly packaged into spores (Type II: 15% in *POL3*$^{-CM}$; 21.7% in *POL3*$^{-AID}$$_{(-IAA)}$) (Fig. 3B and C). Moreover, the amount of unpackaged DNA was generally much higher in the *POL3*$^{-AID}$$_{(+IAA)}$ cells compared to the *POL3*$^{-AID}$$_{(-IAA)}$ cells. Therefore, we inferred that defective chromosome segregation is a common characteristic in the *POL3*$^{-CM}$ and *POL3*$^{-AID}$ cells.

POL3^{-CM} and *POL3*$^{-AID}$ contribute to a recombination defect in CO and NCO formations

DSBs were first detected 2.5 h after the WT cells were transferred to the SPM medium, peaked at ∼3.5 h (6.9% of hybridizing DNA), and had disappeared by 8 h. Comparatively, the DSBs appeared slightly later in the *POL3*$^{-CM}$ and *POL3*$^{-AID}$ cells, which can be attributed to delayed pre-meiotic replication (Fig. 3D and Supplementary Fig. S2D). DSBs in *POL3*$^{-AID}$$_{(+IAA)}$ cells also experienced the same delay after adding auxin. Interestingly, a significant subset of DSBs exhibited a 2–3 h delay in repair in the *POL3*$^{-CM}$ and *POL3*$^{-AID}$ cells, unlike in the *POL3*$^{-AID}$$_{(+IAA)}$ cells (Fig. 3D and E). Therefore, to improve understanding of the involvement of Pol δ in DSB resection, we performed a 2D gel analysis to estimate the ssDNA length at the DSB ends. Notably, the *pol3* hypomorph/degron mutants displayed DSB hyper-resection, resulting in extended ssDNA lengths (Supplementary Fig. S8).

In the *POL3*$^{-CM}$, *POL3*$^{-AID}$$_{(-IAA)}$, and *POL3*$^{-AID}$$_{(+IAA)}$ cells, the levels of CO formation reached ∼61%, 50%, and 16%, respectively, of the levels observed in the WT cells (Fig. 3F and G). This reduction in CO formation is closely linked to the decrease in the IH–dHJ formation in *pol3* mutant cells. The specific second-end capture step during dHJ formation is similar to the annealing process in the synthesis-dependent strand annealing (SDSA) model, leading to NCO formation [22, 40, 54, 55]. In WT cells, the NCOs predominantly peak ∼8 h after induced meiosis, comprising ∼7% of the total hybridizing DNA signals at the *HIS4LEU2* locus (Fig. 3G and H). However, NCO formation was significantly affected in the *POL3*$^{-CM}$, *POL3*$^{-AID}$$_{(-IAA)}$, and *POL3*$^{-AID}$$_{(+IAA)}$ cells, with NCOs reaching only ∼2.7%, 1.9%, and 0.4% of the total hybridizing signals, respectively (Fig. 3G and H). This suggests that the defects in end-primed synthesis caused by Pol δ inactivation result in a failure to form NCOs at levels comparable to those in WT cells.

MRDS tracts by DNA polymerase δ in yeast chromosomal DNA

POL3^{-CM} and *POL3*$^{-AID}$ cells with normal SEI formation displayed strong dHJ defects relative to the WT. A possible explanation for this phenomenon is that Pol δ-mediated DNA synthesis at the 3′ end of DSBs is essential to promote dHJ and NCO formations. To support this hypothesis, we analyzed MRDS tract formation by Pol δ, where meiotic cells were pulse-labeled with BrdU at specific time points and immediately examined using BrdU immunostaining in surface spread preparations (Fig. 4A–C). The SK1 strain of *S. cerevisiae* was genetically modified by introducing two genes to enhance its ability to incorporate BrdU: *HSV-TK* and *hENT1* (Supplementary Table S1; "Materials and methods" section). Meiotic cultures of the WT, *POL3*$^{-CM}$, *POL3*$^{-AID}$, and the DSB-defective *spo11-Y135F* (*spo11-yf*) cells were appropriately pulsed with BrdU and harvested for analysis. The *spo11-yf* culture was used in this study since it had previously eliminated both DSB formation and meiotic recombination while maintaining normal S-phase length [56, 57]. In this study, active DNA replication occurred between 0 and 2 h (Fig. 4D and E, and Supplementary Fig. S9). Correspondingly, during the S-phase pulse periods (0–2 h), the relative abundance of BrdU signals in the chromosome spreads remained constant across all five analyzed cells (Fig. 4D–F). A noticeable increase in BrdU intensity was observed in WT cells during the recombination period (pulses at 3–4, 4–5, and 5–6 h) (Fig. 4D–F). However, the BrdU signal intensity was significantly reduced in the *POL3*$^{-CM}$, *POL3*$^{-AID}$$_{(-IAA)}$, and *POL3* $^{-AID}$$_{(+IAA)}$ cells. Notably, no increase in BrdU intensity was observed in the *spo11-yf* cells during these recombination periods (Fig. 4D–F). The occurrence of MRDS, usually after 3 h, is likely situated in the zygotene/early pachytene phases facilitated by active Pol δ; furthermore,

MRDS can be discerned functionally from pre-meiotic replication.

RPA–ssDNA filaments are accumulated on the pachytene chromosomes in *POL3*$^{-CM}$ and *POL3*$^{-AID}$ mutants

In the WT cells, at the pachytene stage in meiosis, Rec8 appeared as continuous lines or strongly linear rows of foci (e.g. Fig. 5A). Further, RPA foci existed along the axes before synapsis and were visible between the aligned axes and along the pachytene chromosomes (Fig. 5A and B). The correspondence of these cytological features is further supported by mammalian spermatogenesis studies of structured illumination microscopy (SIM), whereby the RPA foci are shown to appear at the inter-axis bridge between synapsing homologs, where homologs initiate coalignment [58]. However, the *POL3*$^{-CM}$ and *POL3*$^{-AID}$ cells exhibited spiked RPA–ssDNA filaments that emerged from the chromosome axes; most RPA signals with ssDNA appeared towards the outside of the chromosome axes in the pachytene and pachytene-like stages (Fig. 5B and Supplementary Fig. S10). Additionally, these RPA signals were highly accumulated on paired chromosomes at pachytene in *POL3*$^{-CM}$, *POL3*$^{-AID}{}_{(\text{-IAA})}$, and *POL3*$^{-AID}{}_{(\text{+IAA})}$ cells, implying that DSBs remain unrepaired in fully formed synaptonemal complexes between the homologs. This phenotype appears to be caused by the large amount of RPA remaining bound to the DSB ends at the recombination site, likely because *POL3*$^{-CM}$ and *POL3*$^{-AID}$ cells are defective in the post-invasion progression of recombination.

Next, we aimed to investigate the turnover of RPA–ssDNA foci during meiotic prophase I in WT, *POL3*$^{-CM}$, and *POL3*$^{-AID}$ cells. Thus, we utilized the *spo11-yf* strain to distinguish whether the observed RPA foci resulted from defective meiotic recombination or premeiotic replication (Fig. 5C). We detected an average of 39.4 ± 5.7 RPA foci in the WT strain at 4 h, which became undetectable after 8 h (Fig. 5C). However, RPA foci were detected starting at 2.5 h in the *spo11-yf* cells, similar to WT, and decreased after 3.5 h, suggesting that RPA marks the pre-meiotic replication site. RPA foci formation occurred in the *POL3*$^{-CM}$ and *POL3*$^{-AID}$ cells at early prophase, similar to the WT, although a significant number of RPA foci persisted for up to 8 h in the *POL3*$^{-CM}$ and *POL3*$^{-AID}$ cells. Notably, the maximum number of RPA foci observed was 76.7 ± 3.3 in *POL3*$^{-CM}$ and 92.9 ± 7.7 in *POL3*$^{-AID}$ (Fig. 5C). Meanwhile, the number of RPA foci increased drastically in the *POL3*$^{-AID}{}_{(\text{+IAA})}$ cells, reaching ∼122.7 ± 11.5. This constituted a >3.1-fold increase compared to the WT levels (Fig. 5C). Moreover, the size of the RPA foci in the *POL3*$^{-CM}$ and *POL3*$^{-AID}$ cells was significantly larger than in WT cells, suggesting the accumulation of extended ssDNA at DSBs (Fig. 5D and E).

CO-designation and simultaneous SC nucleation occur independently of DNA synthesis

Zip3, a meiosis-specific SUMO ligase, plays a key role in regulating the number and distribution of COs along meiotic chromosomes [40, 59, 60]. Consequently, Zip3 focus patterns are expected to reflect the defects in CO formation that happen before this downstream step. Subsequently, we analyzed the Zip3 foci formation in *POL3*$^{-CM}$ and *POL3*$^{-AID}$ cells and observed no significant change (*POL3*$^{-CM}$, *avg. no.* = 40.6; *POL3*$^{-AID}{}_{(\text{-IAA})}$, *avg. no.* = 40.3; *POL3*$^{-AID}{}_{(\text{+IAA})}$, *avg. no.* = 40.7) compared with the WT (n = 40.6; Fig. 6A and B). Most directly, Pol δ strongly colocalizes with Zip3, which promotes CO progression (Fig. 6C and D). Furthermore, the EdU incorporation assay revealed that most MRDSs are defective in the pachytene chromosomes of *POL3*$^{-CM}$, *POL3*$^{-AID}{}_{(\text{-IAA})}$, and *POL3*$^{-AID}{}_{(\text{+IAA})}$ cells (Fig. 6E–H). Additionally, the *POL3*$^{-CM}$, *POL3*$^{-AID}{}_{(\text{-IAA})}$, and *POL3*$^{-AID}{}_{(\text{+IAA})}$ cells exhibited frequencies of synaptonemal complex formation similar to those in WT cells. However, this process was slightly delayed, as observed by staining spread chromosomes with antibodies against Zip1 (Supplementary Fig. S11). These results were consistent with the DNA physical analyses, showing that the DSB-to-SEI transition progressed normally in CO-fated recombination through the ZMM-dependent pathway, independent of MRDS.

DNA polymerase δ supports Rad52-mediated second-end capture

Previous research has highlighted the significance of Rad52 in promoting strand annealing (presented in the Introduction). In the current study, we observed a substantial impact on dHJ levels following the removal of Pol3. Hence, to explore the epistatic relationship between Rad52 and Pol3, both of which play crucial roles in the SEI-to-dHJ transition, we conducted detailed DNA physical analyses of SEIs and dHJs. For this study, we created an *AID* allele of *RAD52*, allowing cells to degrade Rad52 upon auxin addition in a strain with the *POL3*$^{-CM}$ allele. Depleting Rad52 in both *RAD52*$^{-AID}$ and *RAD52*$^{-AID}$ *POL3*$^{-CM}$ cells increased DNA damage sensitivity when cultured on YPD plates containing MMS (Supplementary Fig. S12). In meiotic recombination, eliminating Rad52 proteins in the *POL3*$^{-CM}$ cells had a similar effect to inactivating Pol δ, further emphasizing the earlier role of Pol δ in the formation of dHJs and NCOs, before the involvement of Rad52 (Supplementary Figs S13 and S14).

Discussion

The current study provides strong evidence that DNA Pol δ directly promotes MRDS and plays a critical role in forming dHJs and NCOs during meiotic recombination. Our findings offer new insights into the nature of MRDS *in vivo*, particularly regarding the crucial first-end DNA synthesis during the post-invasion steps. These results significantly advance our understanding of how DNA synthesis-driven recombination events are regulated during meiosis, confirming the essential role of Pol δ in these processes.

DNA polymerase δ primarily extends the invading strand in D-loops for DNA synthesis

Recombination involves diverse modes of DNA synthesis in a D-loop, leading to the formation of various recombination intermediates that DNA polymerases interact with through distinct sets of proteins [36, 61]. Therefore, any DNA polymerase, capable or incapable of displacement synthesis, could be considered a viable candidate for this form of DNA synthesis. Extensive genetic and biochemical studies have highlighted the significant involvement of *S. cerevisiae* and human Pol δ in recombination [30, 31, 62–72]. Meanwhile, experiments in-

volving yeast *pol3* thermosensitive alleles have demonstrated that Pol δ plays a crucial role in recombinational DNA repair and break-induced replication [63, 69]. Moreover, the *pol3-ct* mutant, which causes a short C-terminal deletion in Pol3, exhibits reduced conversion track lengths and COs during meiosis [31]. These results suggest that Pol δ plays a crucial role in meiotic recombination, contributing to both the SDSA and meiotic CO pathways. Our findings in the thymidine incorporation assays also demonstrate that $POL3^{-CM}/POL3^{-AID}$ or Pol3 depletion leads to an inefficient MRDS tract. Thus, DNA Pol δ likely serves as the primary polymerase responsible for extending the invading strand within a Dmc1-mediated D-loop during meiosis.

Pol ε is a high-fidelity polymerase that may be primarily responsible for leading strand replication [36]. In previous genetic studies conducted in budding yeast, the question of whether Pol ε is essential for recombination-associated DNA synthesis in D-loops has remained ambiguous. Therefore, after applying a similar approach to that used for establishing the involvement of Pol δ in recombination, no indications were discovered, either in this study or previously, to support a substantial contribution of Pol ε in the post-invasion steps of recombination [36, 63, 73, 74]. Nevertheless, additional evidence supporting Pol ε participation in recombination has emerged from examining recombination-associated mutations in yeast strains harboring the Pol ε proofreading-deficient allele *pol2-4* [75]. Although the involvement of Pol ε in the first-end synthesis during homologous recombination is improbable, primarily due to the incapacity of Pol ε to perform strand displacement synthesis [35, 36, 73], we cannot disregard the potential involvement of Pol ε in the second-end of DSB or gap filling. These findings suggest possibilities of functional overlap between both polymerases, or could indicate distinct activities between Pol δ and Pol ε, which may contribute to the intricate and coordinated mechanisms in meiotic recombination.

MRDS facilitates post-invasion steps in CO and NCO pathways

Displacement synthesis within the D-loop occurs continuously during recombination, resembling the leading-strand synthesis during DNA replication [36, 37, 76]. In both CO and NCO events, strand annealing occurs between an old strand exposed by 5′ end-resection and a new strand generated through 3′ end-primed synthesis. Consequently, COs and NCOs can display similar heteroduplex patterns (Fig. 7A). We infer that Pol δ inactivation, which affects the MRDS-mediated heteroduplex DNA tracts, could similarly affect second-end annealing in recombination outcomes (Fig. 7A). Thus, Pol δ assumes a central role in recombination-coupled DNA synthesis, demonstrating particular proficiency in extending the 3′ end of the invading strand within the D-loop/SEI and performing the first end synthesis in both CO and NCO pathways (Fig. 7A). A specific basis for the role of MRDS at this stage could be as follows: The single-stranded tail of the first DSB end ("leading strand") forms a D-loop with a homolog partner DNA, undergoes 3′ end-extension through DNA synthesis, and then yields a pre-dHJ structure distal to the extended D-loop with newly synthesized ssDNA, which is now free to capture the single-stranded tail of the second DSB end ("lagging strand") (Fig. 7A).

During CO-related MRDS, DNA synthesis extends the free 3′ end within the SEI (Fig. 7A). Our physical and cytological analyses of *pol3* alleles, which are defective for MRDS, suggest that these represent a viable model for analyzing the transition from SEI to dHJ formation. In this model, Pol δ plays a crucial role in end-primed synthesis within the SEI and facilitates the long extension of the first DSB end, thereby progressing the strand annealing necessary for dHJ formation—a key CO intermediate in meiosis (Fig. 7A). Thus, the absence of active DNA synthesis at the 3′ end of the SEI leads to low levels of dHJs, while the SEI levels remain unaffected. This reduction in dHJs appears to cause a decrease in CO products. We further observed a phenomenon in the physical analysis of *pol δ* mutants where the relative frequency of CO events was higher than that of NCO events. A plausible explanation for this observation could be the formation of three-arm SEIs that do not undergo DNA synthesis. After the extension of D-loop branches during DNA synthesis, the nascent strand can be displaced from the D-loop, leading to helicase-mediated branch migration and the formation of three-arm SEIs [22, 26, 27]. These SEIs could be resolved into half COs through a dHJ lacking a second DNA strand. Furthermore, these three-arm SEI structures exhibit similar molecular weight and migration behaviors as regular SEIs; however, these structures essentially represent dHJs that can subsequently be resolved as half COs along with a broken DNA end [26, 27]. Our results suggest that efficient DNA synthesis at the 3′ end of the first DSB is likely imperative for proper Watson–Crick pairing, which is essential for the second-end capture. This pairing is crucial for ensuring the fidelity of recombination events and preventing potentially deleterious chromosome segregation.

The extension of DNA synthesis primed by the invading 3′ end has emerged as another critical determinant in successful SDSA [77]. During the process of NCOs via SDSA, several developments contribute to the successful annealing of break ends: strand invasion into homolog template DNA, ultimately aiding in the alignment of the homologs; the extent of DNA synthesis primed by the invading the first 3′ end; D-loop disassembly, which terminates DNA synthesis and strand extension [1, 10, 21]. Therefore, proper regulation of D-loop disassembly is crucial to prevent excessive DNA synthesis since an imbalance could lead to outcomes with incomplete repair or aberrant recombination [76]. Our analysis demonstrates the impact of dysfunctional Pol δ on the SDSA pathway by highlighting reductions in both NCO and BrdU incorporation. These reductions provide valuable insights into the defect in MRDS, similar to that observed in CO-related MRDS.

Single-end invasion normally occurs without extension by DNA synthesis

The SEI can undergo CO-designated recombination through dHJs after capturing the second DSB ends [21–27]. Hunter and Kleckner employed a denaturing 2D gel analysis and reported that end-primed synthesis is unnecessary for SEI formation after the first strand invasion [38]. Similarly, our results showed that in *pol3* cells, where DNA synthesis was inactive, SEIs formed at WT levels, providing direct evidence that SEIs can still form without DNA synthesis. Additionally, we observed that SEIs promptly disappeared in the *pol δ* mutants after failing to form dHJs, similar to those observed in

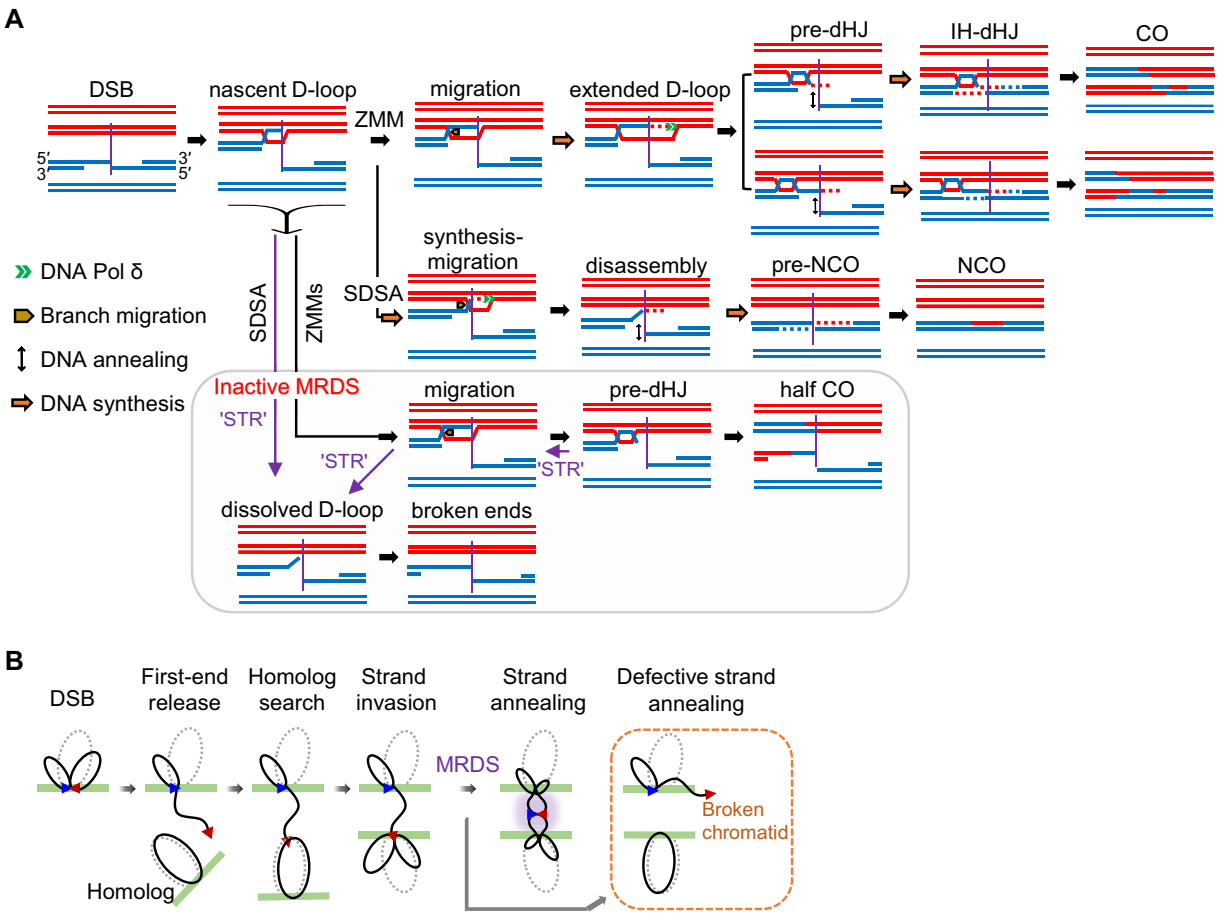

Figure 7. Roles of DNA Pol δ in meiotic recombination. (**A**) Proposed model of MRDS. dHJ and NCO formations require Pol δ-mediated DNA synthesis for the first DSB end extension. For CO formation, the inactivation of Pol δ produces only half the COs through branch migration because the leading strand that is annealed with the second DSB end is not synthesized. Furthermore, when Pol δ is inactivated, the first DSB end might be disassembled without DNA synthesis through the Sgs1–Top3–Rmi1 (STR) helicase–decatenase activity, leading to the failure of NCO formation [78]. Therefore, due to the inactivity of Pol δ, both DSB ends remain unrepaired. (**B**) MRDS in a meiotic chromosome with a tethered-loop axis complex (TLAC). When DSBs occur, the first DSB end (the leading strand) in the TLAC is released to search the homolog template and establish interhomolog interactions through strand invasion. Proteins such as Pol δ, Rad52, and RPA are associated with annealing the lagging strand, and broken chromatids remain when these proteins are deficient.

the WT. These data suggest that homolog interactions are established during the nascent D-loop formation, which subsequently undergoes rapid extension into an SEI, and that active MRDS in the SEI could be specifically essential for facilitating the SEI-to-dHJ transition, particularly during CO formation. The SEI intermediates may also undergo branch migration but fail to complete recombination without first-end synthesis. Our study proposes that the SEIs observed in the *pol3* hypomorph/degron mutants might be displaced and subsequently form either a half CO/DSB end or two distinct DSB ends. Furthermore, considering the abundance and large size of RPA foci observed after Pol3 depletion, it is likely that the nascent and extended D-loop (SEIs) could be resolved to resect DSBs through the helicase–decatenase activity of Sgs1–Top3–Rmi1 [78]. These DSBs may be unproductive and repaired via short SDSA or microhomology-mediated end joining [79, 80]. These repair pathways may not require the rapid extension of the nascent strand, a step that is crucial for the transition from SEIs to dHJs. Instead, other DNA polymerases, capable of performing the necessary DNA synthesis at a slower pace, may facilitate the repair of DSBs without the high-speed extension typically associated with dHJ formation. This hypothesis suggests an alternative repair mechanism that could explain the SEI turnover observed in the mutants, despite their failure to transition to dHJ formation.

DNA synthesis involved in D-loop extension is critical for the strand annealing process in general recombination modes

The RPA–Rad52 association in *S. cerevisiae* ensures the second-end capture process required for SEI-to-dHJ transition and general annealing steps, suggesting that CO and NCO completions require the interplay between RPA and Rad52 [27]. Furthermore, Hunter *et al.* demonstrated that *rad52Δ* cells display WT levels of SEIs and the same turnover rate as WT cells, but with a significant reduction in dHJs [26], resembling the findings observed in our $POL3^{-CM}$ and $POL3^{-AID}$ analyses. Additionally, RPA initially associates with both the first and second DSB ends and localizes to CO sites in the early pachytene phase [27]. Thus, the RPA/DSB ends released locally from the chromosome axis participate in the post-invasion steps of Rad52-mediated DNA annealing, thereby accompanying homolog interaction at meiotic recombination

sites (Fig. 7B). Furthermore, a significant number of RPA–ssDNA signals have been observed along paired pachytene chromosomes in *rad52* or *rfa1* mutants, primarily concentrated on the chromosomal axis, which resembles a barbed shape [27]. Interestingly, a study in human cells also reported elevated levels of RPA-bound ssDNA upon Pol δ knockdown [81]. Moreover, upon the depletion of Pol δ, we detected higher levels of RPA foci as observed in *rad52* or *rfa1* mutants [27], indicating the presence of ssDNA in broken chromatids.

An interpretation of the results obtained from super-resolution microscope imaging and the physical analysis is that MRDS modulation is required to promote the post-invasion process of both the CO- and NCO-designated pathways, which Rad52/RPA could also mediate during meiotic recombination. A proposed mechanism for such an effect can be envisioned in the context of current recombination models. Only one (the "first") DSB end interacts with a homolog partner chromatid, while the second end remains associated with its sister chromatid. After CO-designation, the first end promotes an SEI. The second end remains associated with its sister chromatid until incorporation into the developing recombination complex at the SEI-to-dHJ transition. At this transition stage, Rad52 and RPA play a role at the end of the second DSB, which is required for capturing the SEI; thus, Rad52 and RPA form a CO-fate dHJ during the post-invasion steps. Further, our findings show that Rad52 depletion in *pol δ* mutants resulted in undetectable dHJs and low CO/NCO event levels. Therefore, MRDS is essential for progressing post-invasion steps, particularly before strand annealing mediated by RPA and Rad52.

Conservation of DNA synthesis in meiotic recombination

Previous findings from an electron microscopic autoradiography analysis in adult *Drosophila* oocytes revealed an apparent correlation between DNA synthesis and the formation of SC-associated recombination nodules [82]. The *Drosophila* MCM8 protein, REC, facilitates meiotic recombination at multiple sites, enabling the capture of DNA strand ends to form dHJs, which can be resolved to yield recombination outcomes [83]. Moreover, similar patterns of significant DNA synthesis were observed in mouse spermatocytes and oocytes during zygotene and pachytene stages, with preferential localization along unsynapsed axes and at discrete SC-associated positions [84]. These essential roles of DNA synthesis in recombination interactions were further supported by observations in budding yeast, *Arabidopsis*, and lily [10, 77, 85–88], illustrating the highly conserved nature of DNA synthesis during recombination and the importance of MRDS as a fundamental mechanism for successful recombination events.

Acknowledgements

We thank Nancy Kleckner and the laboratory members for engaging in helpful discussions and comments on this manuscript.

Author contributions: Hyungseok Choi (Conceptualization, Investigation, Formal analysis, Writing—original draft, Writing—review and editing), Jun Seo Lee (Conceptualization, Visualization, Formal analysis, Investigation, Writing—original draft, Writing—review and editing), Soogene Lee (Formal analysis, Investigation, Writing—original draft), Jeong H. Joo (Resources, Investigation, Writing—original draft), Keun P. Kim (Conceptualization, Formal analysis, Supervision, Funding acquisition, Visualization, Writing—original draft, Writing—review and editing).

Supplementary data

Supplementary data is available at NAR online.

Conflict of interest

None declared.

Funding

This work was supported by grants from the National Research Foundation of Korea (NRF) grant funded by the Korean government (MSIT) (RS-2023–00208191; 2022M3A9J4079468; RS-2024-00461596) and Kun-hee Lee Seoul National University Hospital Child Cancer & Rare Disease Project, Republic of Korea (22B-001-0500). Funding to pay the Open Access publication charges for this article was provided by the National Research Foundation of Korea (NRF) grant funded by the Korean government (MSIT) (RS-2023–00208191).

Data availability

The data supporting this article are available within and in the supplementary information. Additional information and requests for resources and reagents can be directed to the corresponding author, Keun Kim (kpkim@cau.ac.kr), who will fulfill these requests.

References

1. Hunter N. Meiotic recombination: the essence of heredity. *Cold Spring Harb Perspect Biol* 2015;**7**:a016618. https://doi.org/10.1101/cshperspect.a016618
2. Zickler D, Kleckner N. Recombination, pairing, and synapsis of homologs during meiosis. *Cold Spring Harb Perspect Biol* 2015;**7**:a016626. https://doi.org/10.1101/cshperspect.a016626
3. Zickler D, Kleckner N. Meiosis: dances between homologs. *Annu Rev Genet* 2023;**57**:1–63. https://doi.org/10.1146/annurev-genet-061323-044915
4. Lam I, Keeney S. Mechanism and regulation of meiotic recombination initiation. *Cold Spring Harb Perspect Biol* 2015;**7**:a016634. https://doi.org/10.1101/cshperspect.a016634
5. Robert T, Nore A, Brun C *et al.* The TopoVIB-like protein family is required for meiotic DNA double-strand break formation. *Science* 2016;**351**:943–9. https://doi.org/10.1126/science.aad5309
6. Vrielynck N, Chambon A, Vezon D *et al.* A DNA topoisomerase VI-like complex initiates meiotic recombination. *Science* 2016;**351**:939–43. https://doi.org/10.1126/science.aad5196
7. Johzuka K, Ogawa H. Interaction of Mre11 and Rad50: two proteins required for DNA repair and meiosis-specific double-strand break formation in Saccharomyces cerevisiae. *Genetics* 1995;**139**:1521–32. https://doi.org/10.1093/genetics/139.4.1521
8. Kanaar R, Hoeijmakers J. Recombination and joining: different means to the same ends. *Genes Funct* 1997;**1**:165–74. https://doi.org/10.1046/j.1365-4624.1997.00016.x

9. Furuse M, Nagase Y, Tsubouchi H *et al.* Distinct roles of two separable in vitro activities of yeast Mre11 in mitotic and meiotic recombination. *EMBO J* 1998;**17**:6412–25. https://doi.org/10.1093/emboj/17.21.6412
10. Terasawa M, Ogawa H, Tsukamoto Y *et al.* Meiotic recombination-related DNA synthesis and its implications for cross-over and non-cross-over recombinant formation. *Proc Natl Acad Sci USA* 2007;**104**:5965–70. https://doi.org/10.1073/pnas.0611490104
11. Zakharyevich K, Ma Y, Tang S *et al.* Temporally and biochemically distinct activities of Exo1 during meiosis: double-strand break resection and resolution of double Holliday junctions. *Mol Cell* 2010;**40**:1001–15. https://doi.org/10.1016/j.molcel.2010.11.032
12. Szostak JW, Orr-Weaver TL, Rothstein RJ *et al.* The double-strand-break repair model for recombination. *Cell* 1983;**33**:25–35. https://doi.org/10.1016/0092-8674(83)90331-8
13. Hotta Y, Ito M, Stern H. Synthesis of DNA during meiosis. *Proc Natl Acad Sci USA* 1966;**56**:1184–91. https://doi.org/10.1073/pnas.56.4.1184
14. Hong S, Sung Y, Yu M *et al.* The logic and mechanism of homologous recombination partner choice. *Mol Cell* 2013;**51**:440–53. https://doi.org/10.1016/j.molcel.2013.08.008
15. Lao JP, Cloud V, Huang CC *et al.* Meiotic crossover control by concerted action of Rad51-Dmc1 in homolog template bias and robust homeostatic regulation. *PLoS Genet* 2013;**9**:e1003978. https://doi.org/10.1371/journal.pgen.1003978
16. Cloud V, Chan YL, Grubb J *et al.* Rad51 is an accessory factor for Dmc1-mediated joint molecule formation during meiosis. *Science* 2012;**337**:1222–5. https://doi.org/10.1126/science.1219379
17. Shinohara M, Gasior SL, Bishop DK *et al.* Tid1/Rdh54 promotes colocalization of rad51 and dmc1 during meiotic recombination. *Proc Natl Acad Sci USA* 2000;**97**:10814–9. https://doi.org/10.1073/pnas.97.20.10814
18. Hayase A, Takagi M, Miyazaki T *et al.* A protein complex containing Mei5 and Sae3 promotes the assembly of the meiosis-specific RecA homolog Dmc1. *Cell* 2004;**119**:927–40. https://doi.org/10.1016/j.cell.2004.10.031
19. Petukhova GV, Pezza RJ, Vanevski F *et al.* The Hop2 and Mnd1 proteins act in concert with Rad51 and Dmc1 in meiotic recombination. *Nat Struct Mol Biol* 2005;**12**:449–53. https://doi.org/10.1038/nsmb923
20. Cho HR, Kong YJ, Hong SG *et al.* Hop2 and Sae3 are required for Dmc1-mediated double-strand break repair via homolog bias during meiosis. *Mol Cells* 2016;**39**:550–6. https://doi.org/10.14348/molcells.2016.0069
21. Kim KP, Weiner BM, Zhang L *et al.* Sister cohesion and structural axis components mediate homolog bias of meiotic recombination. *Cell* 2010;**143**:924–37. https://doi.org/10.1016/j.cell.2010.11.015
22. Ahuja JS, Harvey CS, Wheeler DL *et al.* Repeated strand invasion and extensive branch migration are hallmarks of meiotic recombination. *Mol Cell* 2021;**81**:4258–70. https://doi.org/10.1016/j.molcel.2021.08.003
23. Lynn A, Soucek R, Börner GV. ZMM proteins during meiosis: crossover artists at work. *Chromosome Res* 2007;**15**:591–605. https://doi.org/10.1007/s10577-007-1150-1
24. Allers T, Lichten M Differential timing and control of noncrossover and crossover recombination during meiosis. *Cell* 2001; **106**:47–57. https://doi.org/10.1016/S0092-8674(01)00416-0
25. Allers T, Lichten M. Intermediates of yeast meiotic recombination contain heteroduplex DNA. *Mol Cell* 2001;**8**:225–31. https://doi.org/10.1016/S1097-2765(01)00280-5
26. Lao JP, Oh SD, Shinohara M *et al.* Rad52 promotes postinvasion steps of meiotic double-strand-break repair. *Mol Cell* 2008;**29**:517–24. https://doi.org/10.1016/j.molcel.2007.12.014
27. Joo JH, Hong S, Higashide MT *et al.* RPA interacts with Rad52 to promote meiotic crossover and noncrossover recombination. *Nucleic Acids Res* 2024;**52**:3794–809. https://doi.org/10.1093/nar/gkae083
28. Garbacz MA, Lujan SA, Burkholder AB *et al.* Evidence that DNA polymerase δ contributes to initiating leading strand DNA replication in Saccharomyces cerevisiae. *Nat Commun* 2018;**9**:858. https://doi.org/10.1038/s41467-018-03270-4
29. Fuchs J, Cheblal A, Gasser SM. Underappreciated roles of DNA polymerase δ in replication stress survival. *Trends Genet* 2021;**37**:476–87. https://doi.org/10.1016/j.tig.2020.12.003
30. Sneeden JL, Grossi SM, Tappin I *et al.* Reconstitution of recombination-associated DNA synthesis with human proteins. *Nucleic Acids Res* 2013;**41**:4913–25. https://doi.org/10.1093/nar/gkt192
31. Maloisel L, Bhargava J, Roeder GS. A role for DNA polymerase δ in gene conversion and crossing over during meiosis in *Saccharomyces cerevisiae*. *Genetics* 2004;**167**:1133–42. https://doi.org/10.1534/genetics.104.026260
32. Wilson MA, Kwon Y, Xu Y *et al.* Pif1 helicase and polδ promote recombination-coupled DNA synthesis via bubble migration. *Nature* 2013;**502**:393–6. https://doi.org/10.1038/nature12585
33. Guo X, Hum YF, Lehner K *et al.* Regulation of hetDNA length during mitotic double-strand break repair in yeast. *Mol Cell* 2017;**67**:539–49. https://doi.org/10.1016/j.molcel.2017.07.009
34. Johnson RE, Klassen R, Prakash L *et al.* A major role of DNA polymerase δ in replication of both the leading and lagging DNA strands. *Mol Cell* 2015;**59**:163–75. https://doi.org/10.1016/j.molcel.2015.05.038
35. Ganai RA, Zhang XP, Heyer WD *et al.* Strand displacement synthesis by yeast DNA polymerase ε. *Nucleic Acids Res* 2016;**44**:8229–40. https://doi.org/10.1093/nar/gkw556
36. McVey M, Khodaverdian VY, Meyer D *et al.* Eukaryotic DNA polymerases in homologous recombination. *Annu Rev Genet* 2016;**50**:393–421. https://doi.org/10.1146/annurev-genet-120215-035243
37. Peterson SE, Keeney S, Jasin M. Mechanistic insight into crossing over during mouse meiosis. *Mol Cell* 2020;**78**:1252–63. https://doi.org/10.1016/j.molcel.2020.04.009
38. Hunter N, Kleckner N. The single-end invasion: an asymmetric intermediate at the double-strand break to double-holliday junction transition of meiotic recombination. *Cell* 2001;**106**:59–70. https://doi.org/10.1016/S0092-8674(01)00430-5
39. Schwacha A, Kleckner N. Identification of double Holliday junctions as intermediates in meiotic recombination. *Cell* 1995;**83**:783–91. https://doi.org/10.1016/0092-8674(95)90191-4
40. Börner GV, Kleckner N, Hunter N. Crossover/noncrossover differentiation, synaptonemal complex formation, and regulatory surveillance at the leptotene/zygotene transition of meiosis. *Cell* 2004;**117**:29–45.
41. Lee MS, Higashide MT, Choi H *et al.* The synaptonemal complex central region modulates crossover pathways and feedback control of meiotic double-strand break formation. *Nucleic Acids Res* 2021;**49**:7537–53. https://doi.org/10.1093/nar/gkab566
42. Joo JH, Kang HA, Kim KP *et al.* Meiotic prophase roles of Pds5 in recombination and chromosome condensation in budding yeast. *J Microbiol* 2022;**60**:177–86. https://doi.org/10.1007/s12275-022-1635-9
43. Rhee K, Choi H, Kim KP *et al.* A method for physical analysis of recombination intermediates in *Saccharomyces cerevisiae*. *J Microbiol* 2023;**61**:939–51. https://doi.org/10.1007/s12275-023-00094-w
44. Yoon SW, Lee MS, Xaver M *et al.* Meiotic prophase roles of Rec8 in crossover recombination and chromosome structure. *Nucleic Acids Res* 2016;**44**:9296–314.
45. Kong YJ, Joo JH, Kim KP *et al.* Hed1 promotes meiotic crossover formation in *Saccharomyces cerevisiae*. *J Microbiol Biotechnol* 2017;**27**:405–11. https://doi.org/10.4014/jmb.1610.10074
46. Loidl J, Klein F, Engebrecht J. Genetic and morphological approaches for the analysis of meiotic chromosomes in yeast. *Methods Cell Biol* 1997;**53**:257–85.

47. Lengronne A, Pasero P, Bensimon A *et al.* Monitoring S phase progression globally and locally using BrdU incorporation in TK(+) yeast strains. *Nucleic Acids Res* 2001;**29**:1433–42. https://doi.org/10.1093/nar/29.7.1433
48. Viggiani CJ, Aparicio OM. New vectors for simplified construction of BrdU-incorporating strains of *Saccharomyces cerevisiae*. *Yeast* 2006;**23**:1045–51. https://doi.org/10.1002/yea.1406
49. Lord SJ, Velle KB, Mullins RD *et al.* SuperPlots: communicating reproducibility and variability in cell biology. *J Cell Biol* 2020;**219**:e202001064. https://doi.org/10.1083/jcb.202001064
50. Johansson E, Majka J, Burgers PM. Structure of DNA polymerase δ from *Saccharomyces cerevisiae*. *J Biol Chem* 2001;**276**:43824–8. https://doi.org/10.1074/jbc.M108842200
51. Shimada K, Tsai-Pflugfelder M, Motlagh NDV *et al.* The stabilized Pol31–Pol3 interface counteracts Pol32 ablation with differential effects on repair. *Life Sci Alliance* 2021;**4**:e202101138. https://doi.org/10.26508/lsa.202101138
52. Morawska M, Ulrich HD. An expanded tool kit for the auxin-inducible degron system in budding yeast. *Yeast* 2013;**30**:341–51. https://doi.org/10.1002/yea.2967
53. Oh SD, Lao JP, Taylor AF *et al.* RecQ helicase, Sgs1, and XPF family endonuclease, Mus81–Mms4, resolve aberrant joint molecules during meiotic recombination. *Mol Cell* 2008;**31**:324–36. https://doi.org/10.1016/j.molcel.2008.07.006
54. Oh SD, Lao JP, Hwang PY *et al.* BLM ortholog, Sgs1, prevents aberrant crossing-over by suppressing formation of multichromatid joint molecules. *Cell* 2007;**130**:259–72. https://doi.org/10.1016/j.cell.2007.05.035
55. Hong S, Joo JH, Yun H *et al.* Recruitment of Rec8, Pds5 and Rad61/Wapl to meiotic homolog pairing, recombination, axis formation and S-phase. *Nucleic Acids Res* 2019;**47**:11691–708.
56. Bergerat A, de Massy B, Gadelle D *et al.* An atypical topoisomerase II from Archaea with implications for meiotic recombination. *Nature* 1997;**386**:414–7. https://doi.org/10.1038/386414a0
57. Cha RS, Weiner BM, Keeney S *et al.* Progression of meiotic DNA replication is modulated by interchromosomal interaction proteins, negatively by Spo11p and positively by Rec8p. *Genes Dev* 2000;**14**:493–503. https://doi.org/10.1101/gad.14.4.493
58. Yoon S, Choi EH, Kim JW *et al.* Structured illumination microscopy imaging reveals localization of replication protein A between chromosome lateral elements during mammalian meiosis. *Exp Mol Med* 2018;**50**:1–12.
59. Cheng CH, Lo YH, Liang SS *et al.* SUMO modifications control assembly of synaptonemal complex and polycomplex in meiosis of *Saccharomyces cerevisiae*. *Genes Dev* 2006;**20**:2067–81. https://doi.org/10.1101/gad.1430406
60. Serrentino ME, Chaplais E, Sommermeyer V *et al.* Differential association of the conserved SUMO ligase Zip3 with meiotic double-strand break sites reveals regional variations in the outcome of meiotic recombination. *PLoS Genet* 2013;**9**:e1003416. https://doi.org/10.1371/journal.pgen.1003416
61. McIlwraith MJ, West SC. DNA repair synthesis facilitates RAD52-mediated second-end capture during DSB repair. *Mol Cell* 2008;**29**:510–6. https://doi.org/10.1016/j.molcel.2007.11.037
62. Nick McElhinny SA, Gordenin DA, Stith CM *et al.* Division of labor at the eukaryotic replication fork. *Mol Cell* 2008;**30**:137–44. https://doi.org/10.1016/j.molcel.2008.02.022
63. Fabre F, Boulet A, Faye G. Possible involvement of the yeast POLIII DNA polymerase in induced gene conversion. *Molec Gen Genet* 1991;**229**:353–6. https://doi.org/10.1007/BF00267455
64. Pâques F, Haber JE. Two pathways for removal of nonhomologous DNA ends during double-strand break repair in *Saccharomyces cerevisiae*. *Mol Cell Biol* 1997;**17**:6765–71.
65. Giot L, Chanet R, Simon M *et al.* Involvement of the yeast DNA polymerase δ in DNA repair in vivo. *Genetics* 1997;**146**:1239–51. https://doi.org/10.1093/genetics/146.4.1239
66. Holmes AM, Haber JE. Double-strand break repair in yeast requires both leading and lagging strand DNA polymerases. *Cell* 1999;**96**:415–24. https://doi.org/10.1016/S0092-8674(00)80554-1
67. Wang X, Ira G, Tercero JA *et al.* Role of DNA replication proteins in double-strand break-induced recombination in *Saccharomyces cerevisiae*. *Mol Cell Biol* 2004;**24**:6891–9. https://doi.org/10.1128/MCB.24.16.6891-6899.2004
68. Lydeard JR, Jain S, Yamaguchi M *et al.* Break-induced replication and telomerase-independent telomere maintenance require Pol32. *Nature* 2007;**448**:820–3. https://doi.org/10.1038/nature06047
69. Maloisel L, Fabre F, Gangloff S. DNA polymerase δ is preferentially recruited during homologous recombination to promote heteroduplex DNA extension. *Mol Cell Biol* 2008;**28**:1373–82. https://doi.org/10.1128/MCB.01651-07
70. Li X, Stith CM, Burgers PM *et al.* PCNA is required for initiation of recombination-associated DNA synthesis by DNA polymerase δ. *Mol Cell* 2009;**36**:704–13. https://doi.org/10.1016/j.molcel.2009.09.036
71. Sebesta M, Burkovics P, Haracska L *et al.* Reconstitution of DNA repair synthesis *in vitro* and the role of polymerase and helicase activities. *DNA Repair (Amst)* 2011;**10**:567–76. https://doi.org/10.1016/j.dnarep.2011.03.003
72. Koussa NC, Smith DJ. Limiting DNA polymerase delta alters replication dynamics and leads to a dependence on checkpoint activation and recombination-mediated DNA repair. *PLoS Genet* 2021;**17**:e1009322. https://doi.org/10.1371/journal.pgen.1009322
73. Podust VN, Hübscher U. Lagging strand DNA synthesis by calf thymus DNA polymerases alpha, beta, delta and epsilon in the presence of auxiliary proteins. *Nucl Acids Res* 1993;**21**:841–6. https://doi.org/10.1093/nar/21.4.841
74. Hałas A, Ciesielski A, Zuk J. Involvement of the essential yeast DNA polymerases in induced gene conversion. *Acta Biochim Pol* 1999;**46**:862–72.
75. Hicks WM, Kim M, Haber JE. Increased mutagenesis and unique mutation signature associated with mitotic gene conversion. *Science* 2010;**329**:82–5. https://doi.org/10.1126/science.1191125
76. Vernekar DV, Reginato G, Adam C *et al.* The Pif1 helicase is actively inhibited during meiotic recombination which restrains gene conversion tract length. *Nucleic Acids Res* 2021;**49**:4522–33. https://doi.org/10.1093/nar/gkab232
77. Wang Y, Copenhaver GP. Meiotic recombination: mixing it up in plants. *Annu Rev Plant Biol* 2018;**69**:577–609. https://doi.org/10.1146/annurev-arplant-042817-040431
78. Tang S, Wu MK, Zhang R *et al.* Pervasive and essential roles of the Top3–Rmi1 decatenase orchestrate recombination and facilitate chromosome segregation in meiosis. *Mol Cell* 2015;**57**:607–21. https://doi.org/10.1016/j.molcel.2015.01.021
79. Guo X, Hum YF, Lehner K *et al.* Regulation of hetDNA length during mitotic double-strand break repair in yeast. *Mol Cell* 2017;**67**:539–49. https://doi.org/10.1016/j.molcel.2017.07.009
80. Meyer D, Fu BX, Heyer WD. DNA polymerases δ and λ cooperate in repairing double-strand breaks by microhomology-mediated end-joining in *Saccharomyces cerevisiae*. *Proc Natl Acad Sci USA* 2015;**112**:E6907–16. https://doi.org/10.1073/pnas.1507833112
81. Ercilla A, Benada J, Amitash S *et al.* Physiological tolerance to ssDNA enables strand uncoupling during DNA replication. *Cell Rep* 2020;**30**:2416–29. https://doi.org/10.1016/j.celrep.2020.01.067
82. Carpenter AT. EM autoradiographic evidence that DNA synthesis occurs at recombination nodules during meiosis in *Drosophila melanogaster* females. *Chromosoma* 1981;**83**:59–80. https://doi.org/10.1007/BF00286016
83. Blanton HL, Radford SJ, McMahan S *et al.* REC, Drosophila MCM8, drives formation of meiotic crossovers. *PLoS Genet* 2005;**1**:e40. https://doi.org/10.1371/journal.pgen.0010040
84. Moses MJ, Poorman PA, Dresser ME *et al.* 1985; The synaptonemal complex in meiosis: significance of induced perturbations. In: Dellarco VL, Voytek PE, Hollaender A (eds.), *Aneuploidy: Etiology and Mechanisms*. New York: Plenum Press, 337–52. https://doi.org/10.1007/978-1-4613-2127-9

85. Stern H, Hotta Y. DNA metabolism during pachytene in relation to crossing over. *Genetics* 1974;**78**:227–35. https://doi.org/10.1093/genetics/78.1.227
86. Huang J, Cheng Z, Wang C *et al.* Formation of interference-sensitive meiotic cross-overs requires sufficient DNA leading-strand elongation. *Proc Natl Acad Sci USA* 2015;**112**:12534–9. https://doi.org/10.1073/pnas.1507165112
87. Hernández Sánchez-Rebato M, Schubert V, White CI. Meiotic double-strand break repair DNA synthesis tracts in *Arabidopsis thaliana*. *PLoS Genet* 2024;**20**.e1011197. https://doi.org/10.1371/journal.pgen.1011197
88. Zheng F, Georgescu RE, Li H *et al.* Structure of eukaryotic DNA polymerase δ bound to the PCNA clamp while encircling DNA. *Proc Natl Acad Sci USA* 2020;**117**:30344–53. https://doi.org/10.1073/pnas.2017637117

Received: December 16, 2024. **Revised:** July 3, 2025. **Editorial Decision:** July 6, 2025. **Accepted:** July 8, 2025